CHAPTER 11

Molecular Liquids

The earlier parts of the book have dealt almost exclusively with atomic systems. In this chapter we consider some of the new problems that arise when the theory is broadened to include molecular fluids.

11.1 THE MOLECULAR PAIR DISTRIBUTION FUNCTION

The description of the structure of a homogeneous molecular fluid in terms of particle densities and distribution functions can be developed along lines similar to those followed in the atomic case. The main added complication is the fact that the phase-space probability density for particles with rotational degrees of freedom is not immediately factorisable into kinetic and configurational parts. This problem is very well treated in the book by Gray and Gubbins[1] and we shall not dwell on it here. The final expressions for the molecular distribution functions resemble closely those obtained for atomic fluids, except that all quantities are now functions of the molecular orientations.

In this chapter we shall be concerned almost exclusively with pair correlations. We therefore take as our starting point a suitably generalised form of the definition (2.5.13) of the pair density in a uniform fluid. Let $\mathbf{R}_i$ be the translational coordinates of molecule i and let $\boldsymbol{\Omega}_i$ be the orientation of i in a laboratory-fixed frame of reference. If the molecule is linear, $\boldsymbol{\Omega}_i \equiv (\theta_i, \phi_i)$, where θ_i, ϕ_i are the usual polar angles; if it is non-linear, $\boldsymbol{\Omega}_i \equiv (\theta_i, \phi_i, \chi_i)$, where θ_i, ϕ_i, χ_i are the Euler angles. Then the molecular pair density is defined as

$$\rho^{(2)}(\mathbf{R}, \mathbf{R}', \boldsymbol{\Omega}, \boldsymbol{\Omega}') = \left\langle \sum_{i=1}^{N} \sum_{j \neq i}^{N} \delta(\mathbf{R} - \mathbf{R}_i)\delta(\mathbf{R}' - \mathbf{R}_j)\delta(\boldsymbol{\Omega} - \boldsymbol{\Omega}_i)\delta(\boldsymbol{\Omega}' - \boldsymbol{\Omega}_j) \right\rangle \quad (11.1.1)$$

and the molecular pair distribution function as

$$g(\mathbf{R}_{12}, \boldsymbol{\Omega}_1, \boldsymbol{\Omega}_2) = (\Omega/\rho)^2 \rho^{(2)}(\mathbf{R}_{12}, \boldsymbol{\Omega}_1, \boldsymbol{\Omega}_2) \quad (11.1.2)$$

where $\Omega \equiv \int \mathrm{d}\boldsymbol{\Omega}_i$. The definition of Ω means that

$$\Omega = \iint \mathrm{d}(\cos\theta_i)\, \mathrm{d}\phi_i = 4\pi, \quad \text{if linear} \quad (11.1.3a)$$

$$\Omega = \iiint \mathrm{d}(\cos\theta_i)\,\mathrm{d}\phi_i\,\mathrm{d}\chi_i = 8\pi^2, \quad \text{if non-linear} \tag{11.1.3b}$$

The coordinates $\mathbf{R}_i$ are often taken to be those of the molecular centre of mass or some other point of high symmetry in the molecule, but the choice of molecular "centre" is entirely arbitrary. To simplify the notation it is convenient to use the symbol $i \equiv (\mathbf{R}_i, \boldsymbol{\Omega}_i)$ to denote both the coordinates of the molecular centre and the orientation of molecule i. Thus the molecular pair distribution function will often be written simply as $g(1,2)$ and the molecular pair correlation function as $h(1,2) = g(1,2) - 1$. The functions $e(1,2) = \exp[-\beta v(1,2)]$, $f(1,2) = e(1,2) - 1$ and $y(1,2) = g(1,2)/e(1,2)$ have the same significance as in the atomic case, but are now functions of the orientations $\boldsymbol{\Omega}_1$, $\boldsymbol{\Omega}_2$. Finally, the molecular direct correlation function $c(1,2)$ is related to $h(1,2)$ by a generalisation of the Ornstein–Zernike relation (3.5.12):

$$h(1,2) = c(1,2) + \frac{\rho}{\Omega}\int c(1,3)h(3,2)\,\mathrm{d}3 \tag{11.1.4}$$

Integration of the pair distribution function over the variables $\boldsymbol{\Omega}_1$, $\boldsymbol{\Omega}_2$ yields a function $g_\mathrm{c}(R)$ (with $R \equiv |\mathbf{R}_{12}|$) that describes the radial distribution of molecular centres:

$$g_\mathrm{c}(R) = \frac{1}{\Omega^2}\iint g(\mathbf{R}, \boldsymbol{\Omega}_1, \boldsymbol{\Omega}_2)\,\mathrm{d}\boldsymbol{\Omega}_1\,\mathrm{d}\boldsymbol{\Omega}_2 \equiv \big\langle g(1,2)\big\rangle_{\boldsymbol{\Omega}_1\boldsymbol{\Omega}_2} \tag{11.1.5}$$

Here and elsewhere in this chapter we use angular brackets with subscripts $\boldsymbol{\Omega}_1 \cdots$ to denote an unweighted average over the angles $\boldsymbol{\Omega}_1 \cdots$, i.e.

$$\langle \cdots \rangle_{\boldsymbol{\Omega}_1} \equiv \frac{1}{\Omega}\int \cdots \mathrm{d}\boldsymbol{\Omega}_1 \tag{11.1.6}$$

With this convention the Ornstein–Zernike relation (11.1.4) may be re-expressed as

$$h(1,2) = c(1,2) + \rho\int \big\langle c(1,3)h(3,2)\big\rangle_{\boldsymbol{\Omega}_3}\,\mathrm{d}\mathbf{R}_3 \tag{11.1.7}$$

If $g(1,2)$ is multiplied by some function of the orientations $\boldsymbol{\Omega}_1$, $\boldsymbol{\Omega}_2$ and then integrated over all coordinates of the pair 1 and 2, the result is a quantity that measures the importance of angular correlations of a specific type. Let us suppose that molecule i has an axis of symmetry and let $\mathbf{u}_i$ be a unit vector along that axis. A set of angular order parameters that are of interest both theoretically and experimentally are those defined as

$$\begin{aligned} G_l &= \rho\int \big\langle P_l(\mathbf{u}_1\cdot\mathbf{u}_2)g(\mathbf{R}_{12}, \boldsymbol{\Omega}_1, \boldsymbol{\Omega}_2)\big\rangle_{\boldsymbol{\Omega}_1\boldsymbol{\Omega}_2}\,\mathrm{d}\mathbf{R}_{12} \\ &= \big\langle (N-1)P_l(\mathbf{u}_1\cdot\mathbf{u}_2)\big\rangle \end{aligned} \tag{11.1.8}$$

where $P_l(\cdots)$ denotes a Legendre polynomial. The value of the first-rank order parameter G_1 determines the dielectric constant of a polar fluid, as we show in Section 11.5, while

G_2 is related to a number of measurable quantities, including the integrated intensity of the spectrum observed in depolarised light-scattering experiments.

When the total potential energy of the fluid is a sum of pair terms the internal energy and equation of state can both be written as integrals over $g(1,2)$. The excess internal energy, for example, is given by

$$\begin{aligned}\frac{U^{\mathrm{ex}}}{N} &= \frac{\rho}{2\Omega^2}\iiint v(1,2)g(1,2)\,\mathrm{d}\mathbf{R}_{12}\,\mathrm{d}\boldsymbol{\Omega}_1\,\mathrm{d}\boldsymbol{\Omega}_2 \\ &= 2\pi\rho\int_0^\infty \big\langle v(1,2)g(1,2)\big\rangle_{\boldsymbol{\Omega}_1\boldsymbol{\Omega}_2} R_{12}^2\,\mathrm{d}R_{12} \end{aligned} \tag{11.1.9}$$

which is the molecular analogue of (2.5.20) The corresponding result for the pressure is a generalisation of (2.5.22):

$$\frac{\beta P}{\rho} = 1 - \frac{2\pi\beta\rho}{3}\int_0^\infty \big\langle v'(1,2)g(1,2)\big\rangle_{\boldsymbol{\Omega}_1\boldsymbol{\Omega}_2} R_{12}^3\,\mathrm{d}R_{12} \tag{11.1.10}$$

where the prime denotes differentiation with respect to R_{12} with $\boldsymbol{\Omega}_1$, $\boldsymbol{\Omega}_2$ held constant. Irrespective of whether or not the potential energy is pairwise additive, an argument similar to that leading to (2.6.12) shows that the isothermal compressibility is given by

$$\rho k_{\mathrm{B}} T\chi_T = 1 + \rho\int \big\langle g(1,2)-1\big\rangle_{\boldsymbol{\Omega}_1\boldsymbol{\Omega}_2}\,\mathrm{d}\mathbf{R}_{12} = 1 + \rho\int \big[g_{\mathrm{c}}(R)-1\big]\,\mathrm{d}\mathbf{R} \tag{11.1.11}$$

This result is of particular interest insofar as all reference to angular coordinates has disappeared.

Equations (11.1.9), (11.1.10) and (11.1.11) are identical to their atomic counterparts except for the fact that the pair functions (or products of pair functions) in the integrands are replaced by their unweighted angular averages. Their significance, however, is largely formal. The many-dimensional character of the molecular pair distribution function means that, in general, these results do not represent practical routes to the calculation of thermodynamic properties. The shape of $g(1,2)$ is difficult even to visualise and if progress is to be made the basic problem must be cast in simpler form. Two different approaches have been widely used. In one, which we review in the next section, $g(1,2)$ (or $h(1,2)$) is expanded in a series of suitably chosen, angle-dependent basis functions; in the other, which we discuss in Section 11.3, the fluid structure is described in terms of *site–site distribution functions*. Use of site–site distribution functions is particularly appropriate when the intermolecular potential is cast in site–site form, as in (1.2.6).

11.2 EXPANSIONS OF THE PAIR DISTRIBUTION FUNCTION

The pair distribution function for molecules of arbitrary symmetry can be expanded in terms of the Wigner rotation matrices or generalised spherical harmonics.[2] The general formalism has not been widely used, however, and the discussion that follows is limited

to linear molecules. In this case the natural expansion functions are the usual spherical harmonics, which we denote by $Y_{lm}(\theta, \phi)$.[3] Let $\boldsymbol{\Omega}_1$, $\boldsymbol{\Omega}_2$ be the orientations of molecules 1, 2 in a system of polar coordinates in which the z-axis lies along the vector $\mathbf{R}_{12} = \mathbf{R}_2 - \mathbf{R}_1$ (the "intermolecular" frame). Then $g(1,2)$ may be written as

$$g(1,2) = 4\pi \sum_{l_1} \sum_{l_2} \sum_{m} g_{l_1 l_2 m}(R) Y_{l_1 m}(\boldsymbol{\Omega}_1) Y_{l_2 \bar{m}}(\boldsymbol{\Omega}_2) \tag{11.2.1}$$

where $R \equiv |\mathbf{R}_{12}|$ and $\bar{m} \equiv -m$. The sum on m runs from $-l$ to l, where l is the lesser of l_1 and l_2; the indices m of the two harmonics are equal (apart from sign) by virtue of the cylindrical symmetry with respect to the axis $\mathbf{R}_{12}$. Important properties of the spherical harmonics include the fact that they are normalised and orthogonal:

$$\int Y^*_{lm}(\boldsymbol{\Omega}) Y_{l'm'}(\boldsymbol{\Omega}) \, \mathrm{d}\boldsymbol{\Omega} = \delta_{ll'} \delta_{mm'} \tag{11.2.2}$$

and that $Y_{l\bar{m}}(\boldsymbol{\Omega}) = (-1)^m Y^*_{lm}(\boldsymbol{\Omega})$.

If (11.2.1) is multiplied through by $Y^*_{l_1 \bar{m}}(\boldsymbol{\Omega}_1) Y^*_{l_2 m}(\boldsymbol{\Omega}_2)$ and integrated over angles, it follows from the properties just quoted that

$$\begin{aligned} g_{l_1 l_2 m}(R) &= \frac{1}{4\pi} \iint Y_{l_1 \bar{m}}(\boldsymbol{\Omega}_1) Y_{l_2 m}(\boldsymbol{\Omega}_2) g(1,2) \, \mathrm{d}\boldsymbol{\Omega}_1 \, \mathrm{d}\boldsymbol{\Omega}_2 \\ &= 4\pi \left\langle Y_{l_1 \bar{m}}(\boldsymbol{\Omega}_1) Y_{l_2 m}(\boldsymbol{\Omega}_2) g(1,2) \right\rangle_{\boldsymbol{\Omega}_1 \boldsymbol{\Omega}_2} \end{aligned} \tag{11.2.3}$$

The expansion coefficients $g_{l_1 l_2 m}(R)$ are called the "projections" of $g(1,2)$ onto the corresponding angular functions and are easily calculated by computer simulation. Certain projections of $g(1,2)$ are closely related to quantities introduced in Section 11.1. Given that $Y_{00}(\boldsymbol{\Omega}) = (1/4\pi)^{1/2}$, we see that $g_{000}(R)$ is identical to the centres distribution function $g_c(R)$; this is the reason for the inclusion of the factor 4π in (11.2.1). Moreover, the order parameters defined by (11.1.8) can be re-expressed as

$$G_l = \frac{\rho}{2l+1} \sum_m (-1)^m \int g_{llm}(R) \, \mathrm{d}\mathbf{R} \tag{11.2.4}$$

This result is a consequence of the addition theorem for spherical harmonics, i.e.

$$P_l(\cos \gamma_{12}) = \frac{4\pi}{2l+1} \sum_m Y^*_{lm}(\boldsymbol{\Omega}_1) Y_{lm}(\boldsymbol{\Omega}_2) \tag{11.2.5}$$

where γ_{12} is the angle between two vectors with orientations $\boldsymbol{\Omega}_1$ and $\boldsymbol{\Omega}_2$.

An expansion similar to (11.2.1) can be made of any scalar function of the variables $\mathbf{R}_{12}$, $\boldsymbol{\Omega}_1$ and $\boldsymbol{\Omega}_2$, including both the intermolecular potential $v(1,2)$ and its derivative with respect to R_{12}. The corresponding expansion coefficients $v_{l_1 l_2 m}(R)$ and $v'_{l_1 l_2 m}(R)$ can be calculated numerically for any pair potential and in some cases are expressible in analytical

form. If we introduce the expansions of $g(1,2)$ and $v(1,2)$ into (11.1.9) and integrate over angles, the energy equation becomes

$$\frac{U^{\text{ex}}}{N} = 2\pi\rho \sum_{l_1}\sum_{l_2}\sum_{m} \int_0^\infty v_{l_1 l_2 m}(R) g_{l_1 l_2 m}(R) R^2 \, \mathrm{d}R \tag{11.2.6}$$

The pressure equation (11.1.10) can be similarly rewritten in terms of the coefficients $v'_{l_1 l_2 m}(R)$ and $g_{l_1 l_2 m}(R)$. The multidimensional integrals appearing on the right-hand sides of (11.1.9) and (11.1.10) are thereby transformed into infinite sums of one-dimensional integrals. In general, however, the new expressions do not represent an improvement in the computational sense. The evidence from Monte Carlo calculations for systems of diatomic molecules is that on the whole the rate of convergence of the sums is poor and becomes rapidly worse as the elongation of the molecule increases.[4]

A different expansion of $g(1,2)$ is obtained if the orientations $\boldsymbol{\Omega}_1$, $\boldsymbol{\Omega}_2$ are referred to a laboratory-fixed frame of reference (the "laboratory" frame). Let $\boldsymbol{\Omega}_R$ be the orientation of the vector $\mathbf{R}_{12}$ in the laboratory frame. Then $g(1,2)$ may be expanded in the form

$$\begin{aligned} g(1,2) = &\sum_{l_1}\sum_{l_2}\sum_{l} g(l_1 l_2 l;\, R) \sum_{m_1}\sum_{m_2}\sum_{m} C(l_1 l_2 l;\; m_1 m_2 m) \\ &\times Y_{l_1 m_1}(\boldsymbol{\Omega}_1) Y_{l_2 m_2}(\boldsymbol{\Omega}_2) Y^*_{lm}(\boldsymbol{\Omega}_R) \end{aligned} \tag{11.2.7}$$

where $C(\cdots)$ is a Clebsch–Gordan coefficient. The coefficients $g(l_1 l_2 l;\; R)$ are linear combinations of the coefficients in (11.2.1) and the two expansions are equivalent if the z-axis of the laboratory frame is taken parallel to $\mathbf{R}_{12}$. The relation between the two sets of coefficients is

$$g(l_1 l_2 l;\; R) = \left(\frac{64\pi^3}{2l+1}\right)^{1/2} \sum_{m} C(l_1 l_2 l;\; m\bar{m}0) g_{l_1 l_2 m}(R) \tag{11.2.8}$$

with, as a special case, $g(000;\; R) = (4\pi)^{3/2} g_{000}(R)$. Equation (11.2.7) is sometimes written in the abbreviated form

$$g(1,2) = \sum_{l_1}\sum_{l_2}\sum_{l} g(l_1 l_2 l;\; R) \Phi^{l_1 l_2 l}(\boldsymbol{\Omega}_1, \boldsymbol{\Omega}_2, \boldsymbol{\Omega}_R) \tag{11.2.9}$$

where $\Phi^{l_1 l_2 l}$ is a "rotational invariant".

Use of (11.2.7) in preference to (11.2.1) does not help in resolving the problem of slow convergence in expansions such as (11.2.6), but it does have some advantages, particularly in the manipulation of Fourier transforms. We shall use the notation $\hat{g}(1,2) \equiv \hat{g}(\mathbf{k}, \boldsymbol{\Omega}_1, \boldsymbol{\Omega}_2)$ to denote a Fourier transform with respect to $\mathbf{R}_{12}$, i.e.

$$\hat{g}(\mathbf{k}, \boldsymbol{\Omega}_1, \boldsymbol{\Omega}_2) = \int g(\mathbf{R}_{12}, \boldsymbol{\Omega}_1, \boldsymbol{\Omega}_2) \exp(-i\mathbf{k}\cdot\mathbf{R}_{12}) \, \mathrm{d}\mathbf{R}_{12} \tag{11.2.10}$$

Then $\hat{g}(1,2)$ can be written in terms of laboratory-frame harmonics as

$$\hat{g}(1,2) = \sum_{l_1}\sum_{l_2}\sum_{l} g(l_1 l_2 l;\ k) \sum_{m_1}\sum_{m_2}\sum_{m} C(l_1 l_2 l;\ m_1 m_2 m) \times Y_{l_1 m_1}(\boldsymbol{\Omega}_1) Y_{l_2 m_2}(\boldsymbol{\Omega}_2) Y^*_{lm}(\boldsymbol{\Omega}_k) \tag{11.2.11}$$

where $\boldsymbol{\Omega}_k$ is the orientation of $\mathbf{k}$ in the laboratory frame. The reason that this expansion and the corresponding expansions of $\hat{h}(1,2)$ and $\hat{c}(1,2)$ are so useful is the fact that the coefficients $g(l_1 l_2 l;\ k)$ and $g(l_1 l_2 l;\ R)$ are related by a generalised Fourier or Hankel transform, i.e.

$$g(l_1 l_2 l;\ k) = 4\pi i^l \int_0^\infty j_l(kR) g(l_1 l_2 l;\ R) R^2\, \mathrm{d}R \tag{11.2.12}$$

where $j_l(\cdots)$ is the spherical Bessel function of order l. No equivalent simplification is found in the case of the intermolecular-frame expansion. We shall not give a general proof of (11.2.12), since in this book we are concerned only with $l = 0$ and $l = 2$. The case when $l = 0$ corresponds to the usual Fourier transform of a spherically symmetric function; the case when $l = 2$ is considered in detail in Section 11.4.

Expansions of $g(1,2)$ and other pair functions along the lines of (11.2.1) and (11.2.7) have been applied most successfully in the theory of polar fluids, as we shall see in Sections 11.5 and 11.6.

11.3 SITE–SITE DISTRIBUTION FUNCTIONS

When an interaction-site model is used to represent the intermolecular potential the natural way to describe the structure of the fluid is in terms of site–site distribution functions. If the coordinates of site α on molecule i are denoted by $\mathbf{r}_{i\alpha}$ and those of site β on molecule j ($j \neq i$) by $\mathbf{r}_{j\beta}$, then the site–site pair distribution function $g_{\alpha\beta}(r)$ is defined in a manner similar to (2.5.15):

$$\begin{aligned} \rho g_{\alpha\beta}(r) &= \left\langle \frac{1}{N} \sum_{i=1}^{N} \sum_{j\neq i}^{N} \delta(\mathbf{r} + \mathbf{r}_{2\beta} - \mathbf{r}_{1\alpha}) \right\rangle \\ &= \left\langle (N-1)\delta(\mathbf{r} + \mathbf{r}_{2\beta} - \mathbf{r}_{1\alpha}) \right\rangle \end{aligned} \tag{11.3.1}$$

The corresponding site–site pair correlation function is defined as $h_{\alpha\beta}(r) = g_{\alpha\beta}(r) - 1$. The site–site distribution functions are, of course, of interest in a wider context than that of interaction-site models. For any real molecular fluid the most important site–site distribution functions are those that describe the distribution of atomic sites.

The definition (11.3.1) can be used to relate the site–site distribution functions to the molecular pair distribution function $g(1,2)$. Let $\boldsymbol{\ell}_{i\alpha}$ be the vector displacement of site α in molecule i from the molecular centre $\mathbf{R}_i$, i.e.

$$\boldsymbol{\ell}_{i\alpha} = \mathbf{r}_{i\alpha} - \mathbf{R}_i \tag{11.3.2}$$

Then $g_{\alpha\beta}(r)$ is given by the integral of $g(1,2)$ over all coordinates, subject to the constraint that the vector separation of sites α, β is equal to $\mathbf{r}$:

$$\begin{aligned} g_{\alpha\beta}(\mathbf{r}) &= \frac{1}{\Omega^2}\iiiint \mathrm{d}\mathbf{R}_1\,\mathrm{d}\mathbf{R}_2\,\mathrm{d}\boldsymbol{\Omega}_1\,\mathrm{d}\boldsymbol{\Omega}_2\,g(1,2) \\ &\quad\times\delta\big[\mathbf{R}_1+\boldsymbol{\ell}_{1\alpha}(\boldsymbol{\Omega}_1)\big]\delta\big[\mathbf{R}_2+\boldsymbol{\ell}_{2\beta}(\boldsymbol{\Omega}_2)-\mathbf{r}\big] \\ &= \frac{1}{\Omega^2}\iiint \mathrm{d}\mathbf{R}_{12}\,\mathrm{d}\boldsymbol{\Omega}_1\,\mathrm{d}\boldsymbol{\Omega}_2\,g(1,2) \\ &\quad\times\delta\big[\mathbf{R}_{12}+\boldsymbol{\ell}_{2\beta}(\boldsymbol{\Omega}_2)-\boldsymbol{\ell}_{1\alpha}(\boldsymbol{\Omega}_1)-\mathbf{r}\big] \end{aligned} \tag{11.3.3}$$

It follows from (11.3.3) that the Fourier transform of $g_{\alpha\beta}(\mathbf{r})$ with respect to $\mathbf{r}$ is

$$\begin{aligned} \hat{g}_{\alpha\beta}(\mathbf{k}) &= \frac{1}{\Omega^2}\iiiint \mathrm{d}\mathbf{R}_{12}\,\mathrm{d}\boldsymbol{\Omega}_1\,\mathrm{d}\boldsymbol{\Omega}_2\,g(1,2) \\ &\quad\times\delta\big[\mathbf{R}_{12}+\boldsymbol{\ell}_{2\beta}(\boldsymbol{\Omega}_2)-\boldsymbol{\ell}_{1\alpha}(\boldsymbol{\Omega}_1)-\mathbf{r}\big]\exp(-i\mathbf{k}\cdot\mathbf{r})\,\mathrm{d}\mathbf{r} \\ &= \frac{1}{\Omega^2}\iiint \mathrm{d}\mathbf{R}_{12}\,\mathrm{d}\boldsymbol{\Omega}_1\,\mathrm{d}\boldsymbol{\Omega}_2\,g(1,2)\exp(-i\mathbf{k}\cdot\mathbf{R}_{12}) \\ &\quad\times\exp\big[-i\mathbf{k}\cdot\boldsymbol{\ell}_{2\beta}(\boldsymbol{\Omega}_2)\big]\exp\big[i\mathbf{k}\cdot\boldsymbol{\ell}_{1\alpha}(\boldsymbol{\Omega}_1)\big] \\ &= \big\langle\hat{g}(1,2)\exp\big[-i\mathbf{k}\cdot\boldsymbol{\ell}_{2\beta}(\boldsymbol{\Omega}_2)\big]\exp\big[i\mathbf{k}\cdot\boldsymbol{\ell}_{1\alpha}(\boldsymbol{\Omega}_1)\big]\big\rangle_{\boldsymbol{\Omega}_1\boldsymbol{\Omega}_2} \end{aligned} \tag{11.3.4}$$

where $\hat{g}(1,2)$ is defined by (11.2.10). There is an analogous expression for $\hat{h}_{\alpha\beta}(\mathbf{k})$ in terms of $h(1,2)$.

The site–site distribution functions have a simple physical interpretation. They are also directly related to the structure factors measured in x-ray and neutron-scattering experiments. On the other hand, the integrations in (11.3.3) involve an irretrievable loss of information, and $g(1,2)$ cannot be reconstructed exactly from any finite set of site–site distribution functions.

Many of the quantities that are expressible as integrals over $g(1,2)$ can also be written in terms of site–site distribution functions. For example, if the intermolecular potential is of the interaction-site form and the site–site potentials are spherically symmetric, the excess internal energy is given by

$$\frac{U^{\mathrm{ex}}}{N} = 2\pi\rho\sum_{\alpha}\sum_{\beta}\int_0^{\infty} v_{\alpha\beta}(r)g_{\alpha\beta}(r)r^2\,\mathrm{d}r \tag{11.3.5}$$

Equation (11.3.5) is a straightforward generalisation of (2.5.20) and can be derived by the same intuitive approach discussed in connection with the earlier result. The generalisation of the virial equation (2.5.22) is more complicated and knowledge of $g_{\alpha\beta}(r)$ for all α, β is not sufficient to determine the pressure. The equation of state can, however, be determined by integration of the compressibility equation (11.1.11). Because the choice of molecular

centre is arbitrary, and need not be the same for each molecule, (11.1.11) can be written as

$$\rho k_{\mathrm{B}} T \chi_T = 1 + \rho \int \left[g_{\alpha\beta}(r) - 1 \right] \mathrm{d}\mathbf{r} = 1 + \rho \hat{h}_{\alpha\beta}(0) \tag{11.3.6}$$

where α, β refer to any pair of sites. Finally, the angular correlation parameters G_l defined by (11.1.8) can be expressed[5] as integrals over combinations of the functions $h_{\alpha\beta}(r)$. In the case of a heteronuclear but non-polar molecule with atomic sites α and β the result for G_1 is[6]

$$G_1 = -\frac{\rho}{2L^2} \int_0^\infty r^2 \Delta h(r) \, \mathrm{d}\mathbf{r} \tag{11.3.7}$$

where L is the bondlength and

$$\Delta h(r) = h_{\alpha\alpha}(r) + h_{\beta\beta}(r) - 2h_{\alpha\beta}(r) \tag{11.3.8}$$

If $\hat{h}_{\alpha\beta}(k)$ is expanded in powers of k in the form

$$\hat{h}_{\alpha\beta}(k) = 4\pi \int_0^\infty h_{\alpha\beta}(r) \frac{\sin kr}{kr} r^2 \, \mathrm{d}r = \hat{h}_{\alpha\beta}(0) + h^{(2)}_{\alpha\beta} k^2 + \cdots \tag{11.3.9}$$

we find that G_1 is proportional to the coefficient of k^2 in the small-k expansion of $\Delta\hat{h}(k)$:

$$G_1 = \frac{3\rho}{L^2} \Delta h^{(2)} \tag{11.3.10}$$

Similarly, G_l for $l > 1$ can be written in terms of the higher-order coefficients $\Delta h^{(n)}$. The example given is somewhat artificial, since any real heteronuclear molecule will have a dipole moment; in that case (11.3.7) is no longer correct. Nonetheless, it serves to illustrate the general form of the results, and we shall see in Section 11.5 how (11.3.7) can be recovered from the expression appropriate to polar molecules. If the molecule is homonuclear, all site–site distribution functions are the same and G_1 vanishes, as it must do on grounds of symmetry.

Information on the atom–atom distribution functions of real molecules is gained experimentally from the analysis of radiation-scattering experiments. Consider first the case of a homonuclear diatomic. Let $\mathbf{u}_i$ be a unit vector along the internuclear axis of molecule i. Then the coordinates of atoms α, β relative to the centre of mass $\mathbf{R}_i$ are

$$\mathbf{r}_{i\alpha} = \mathbf{R}_i + \tfrac{1}{2}\mathbf{u}_i L, \qquad \mathbf{r}_{i\beta} = \mathbf{R}_i - \tfrac{1}{2}\mathbf{u}_i L \tag{11.3.11}$$

We define the Fourier components of the atomic density as

$$\rho_{\mathbf{k}} = \sum_{i=1}^{N} \left[\exp(-i\mathbf{k} \cdot \mathbf{r}_{i\alpha}) + \exp(-i\mathbf{k} \cdot \mathbf{r}_{i\beta}) \right] \tag{11.3.12}$$

and the molecular structure factor as

$$S(k) = \left\langle \frac{1}{4N} \rho_{\mathbf{k}} \rho_{-\mathbf{k}} \right\rangle \tag{11.3.13}$$

where N is the number of molecules. The factor $\frac{1}{4}$ is included in order to make the definition of $S(k)$ reduce to that of an atomic fluid in the limit $L \to 0$. The statistical average in (11.3.13) may be rewritten in terms of either the atomic or molecular pair distribution functions. In the first case, by exploiting the fact that atoms α, β in each molecule play equivalent roles, we can write

$$\left\langle \frac{1}{4N} \rho_{\mathbf{k}} \rho_{-\mathbf{k}} \right\rangle = \frac{1}{2} + \frac{1}{2N} \sum_{i=1}^{N} \left\langle \cos(\mathbf{k} \cdot \mathbf{u}_i L) \right\rangle_{\boldsymbol{\Omega}_i} + \left\langle \frac{1}{4N} \sum_{i=1}^{N} \sum_{j \neq i}^{N} \exp\left[-i\mathbf{k} \cdot (\mathbf{r}_{j\beta} - \mathbf{r}_{i\alpha}) \right] \right\rangle \tag{11.3.14}$$

The second term on the right-hand side involves only an average over angles and the third term can be related to any of the four identical distribution functions $g_{\alpha\beta}(r)$ via the definition (11.3.1). Thus

$$S(k) = S_{\text{intra}}(k) + S_{\text{inter}}(k) \tag{11.3.15}$$

The first term on the right-hand side of (11.3.15) is the intramolecular contribution:

$$S_{\text{intra}}(k) = \tfrac{1}{2}\left(1 + \langle \cos \mathbf{k} \cdot \mathbf{u}_i L \rangle_{\boldsymbol{\Omega}_i}\right) = \tfrac{1}{2}\left[1 + j_0(kL)\right] \tag{11.3.16}$$

where $j_0(x) = x^{-1} \sin x$. The intermolecular part is given by

$$S_{\text{inter}}(k) = \rho \int h_{\alpha\beta}(r) \exp(-i\mathbf{k} \cdot \mathbf{r}) \, \mathrm{d}\mathbf{r} = S_{\alpha\beta}(k) - 1 \tag{11.3.17}$$

where $S_{\alpha\beta}(k)$ is the atomic structure factor and a physically unimportant term in $\delta(\mathbf{k})$ has been omitted. The total intensity of scattered radiation at a given value of k is proportional to the structure factor (11.3.15); this can be inverted to yield the atomic pair distribution function if the intramolecular part is first removed.[7]

In order to relate $S(k)$ to the molecular pair distribution function we start from the definition (11.3.13) and proceed as follows:

$$\begin{aligned} S(k) &= \left\langle \frac{1}{4N} \rho_{\mathbf{k}} \rho_{-\mathbf{k}} \right\rangle \\ &= \left\langle \frac{1}{N} \sum_{i=1}^{N} \sum_{j=1}^{N} \exp(-i\mathbf{k} \cdot \mathbf{R}_{ij}) \cos\left(\tfrac{1}{2}\mathbf{k} \cdot \mathbf{u}_i L\right) \cos\left(\tfrac{1}{2}\mathbf{k} \cdot \mathbf{u}_j L\right) \right\rangle \\ &= \tfrac{1}{2}\left[1 + j_0(kL)\right] \end{aligned}$$

$$+\left\langle \frac{1}{N}\sum_{i=1}^{N}\sum_{j\neq i}^{N}\exp(-i\mathbf{k}\cdot\mathbf{R}_{ij})\cos\left(\tfrac{1}{2}\mathbf{k}\cdot\mathbf{u}_i L\right)\cos\left(\tfrac{1}{2}\mathbf{k}\cdot\mathbf{u}_j L\right)\right\rangle$$

$$= S_{\text{intra}}(k) + \frac{\rho}{\Omega^2}\iiint \left[g(1,2)-1\right]\exp(-i\mathbf{k}\cdot\mathbf{R}_{12})$$

$$\times \cos\left(\tfrac{1}{2}\mathbf{k}\cdot\mathbf{u}_1 L\right)\cos\left(\tfrac{1}{2}\mathbf{k}\cdot\mathbf{u}_2 L\right)\mathrm{d}\mathbf{R}_{12}\,\mathrm{d}\boldsymbol{\Omega}_1\,\mathrm{d}\boldsymbol{\Omega}_2 \tag{11.3.18}$$

Equation (11.3.18) is an exact relation between $S(k)$ and $g(1,2)$. Comparison with (11.3.4) shows that the second term on the right-hand side is $\hat{h}_{\alpha\beta}(k)$; this can also be deduced from inspection of Eqns (11.3.15) to (11.3.17). A more tractable expression is obtained by replacing $g(1,2)$ by it spherical-harmonic expansion (11.2.1). The structure factor can then be written as

$$S(k) = S_{\text{intra}}(k) + f(k)\left[S_{\text{c}}(k)-1\right] + S_{\text{aniso}}(k) \tag{11.3.19}$$

where

$$f(k) = \left\langle \cos\left(\tfrac{1}{2}\mathbf{k}\cdot\mathbf{u}_1 L\right)\cos\left(\tfrac{1}{2}\mathbf{k}\cdot\mathbf{u}_2 L\right)\right\rangle_{\boldsymbol{\Omega}_1\boldsymbol{\Omega}_2} = \left[j_0\left(\tfrac{1}{2}kL\right)\right]^2 \tag{11.3.20}$$

and $S_{\text{c}}(k)$ is the Fourier transform of the centres distribution function $g_{\text{c}}(r)$. The term $S_{\text{aniso}}(k)$ in (11.3.19) represents the contribution to $S(k)$ from the angle-dependent terms in $g(1,2)$, i.e. from all spherical harmonics beyond $(l_1, l_2, m) = (0,0,0)$. If the intermolecular potential is only weakly anisotropic, $S_{\text{aniso}}(k)$ will be small. In those circumstances it follows from (11.3.15), (11.3.17) and (11.3.19) that

$$S_{\alpha\beta}(k) \approx 1 + f(k)\left[S_{\text{c}}(k)-1\right] \tag{11.3.21}$$

Equation (11.3.21) is called the "free-rotation" approximation. This can be expected to work well only when the intermolecular potential is very weakly anisotropic, as in the case of liquid nitrogen, for example. At the same time, even in the absence of strong orientational correlations, the modulating role of the function $f(k)$ means that the intermolecular contribution to $S(k)$ will differ from the structure factor of an atomic fluid. This is evident in Figure 11.1, which shows the results of x-ray scattering experiments on liquid nitrogen. Although the function $S_{\text{c}}(k)$ cannot usually be determined experimentally,[9] the evidence from computer simulations[10] is that for small molecules it has a strongly oscillatory character and can be well fitted by the structure factor of an atomic system. By contrast, as comparison of Figures 3.2 (or 5.1) and 11.1 reveals, the first peak in the molecular structure factor is significantly weaker and the later oscillations are more strongly damped than in the case of a typical atomic fluid. Note also that beyond the first peak the behaviour of the molecular structure factor is dominated by the intramolecular term. The free-rotation approximation becomes exact in the limit $k \to 0$ because the cosine terms in (11.3.18) all approach unity. Thus

$$\rho k_{\text{B}} T \chi_T = \lim_{k\to 0} S(k) = 1 + \rho\int \left[g_{\text{c}}(R)-1\right]\mathrm{d}\mathbf{R} \tag{11.3.22}$$

which is the same result as in (11.1.11).

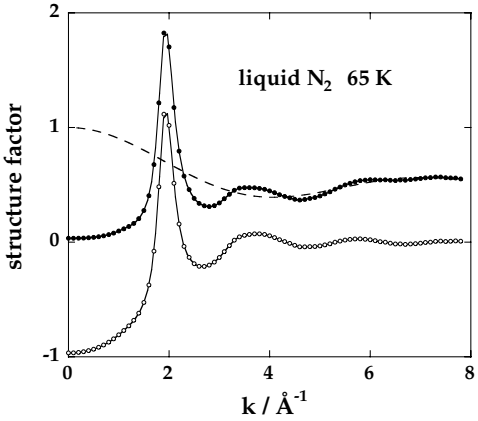

FIG. 11.1. Results obtained by x-ray scattering for the structure factor of liquid nitrogen near its triple point. Filled circles: $S(k)$; open circles: $S_{\text{inter}}(k)$; dashes: $S_{\text{intra}}(k)$. After Narten *et al.*[8]

For heteronuclear molecules there is normally little value in defining a structure factor through a formula analogous to (11.3.13). It is more useful instead to focus attention on those combinations of atomic structure factors that are experimentally accessible. In the case of neutron scattering the measured structure factor can again be written in the form of (11.3.15), but now

$$\left(\sum_\alpha b_\alpha\right)^2 S^{\text{N}}_{\text{intra}}(k) = \sum_\alpha b_\alpha^2 + \sum_\alpha \sum_{\beta\neq\alpha} b_\alpha b_\beta j_0(kL_{\alpha\beta}) \tag{11.3.23a}$$

$$\begin{aligned}\left(\sum_\alpha b_\alpha\right)^2 S^{\text{N}}_{\text{inter}}(k) &= \rho \sum_\alpha \sum_\beta b_\alpha b_\beta \int \big[g_{\alpha\beta}(r) - 1\big] \exp(-i\mathbf{k}\cdot\mathbf{r})\, \mathrm{d}\mathbf{r} \\ &= \sum_\alpha \sum_\beta b_\alpha b_\beta \big[S_{\alpha\beta}(k) - 1\big]\end{aligned} \tag{11.3.23b}$$

where the sums run over all nuclei in the molecule, b_α is the coherent neutron scattering length of nucleus α and $L_{\alpha\beta}$ is the separation of nuclei α, β. These expressions reduce to (11.3.16) and (11.3.17) for a diatomic molecule with $b_\alpha = b_\beta$. After removal of the intramolecular term, Fourier transformation yields a weighted sum of atomic pair distribution functions of the form

$$g^{\text{N}}(r) = \sum_\alpha \sum_\beta b_\alpha b_\beta g_{\alpha\beta}(r) \Big/ \left(\sum_\alpha b_\alpha\right)^2 \tag{11.3.24}$$

Isotopic substitution makes it possible to vary the weights with which the different $g_{\alpha\beta}(r)$ contribute to $g^{\text{N}}(r)$ and hence, in favourable cases, to determine some or all of the individual atom–atom distribution functions.

Formulae similar to (11.3.23) apply also to x-ray scattering, the only difference being that the nuclear scattering lengths are replaced by the atomic form factors (see Section 4.1). Since the form factors are functions of k, the weighted distribution function $g^{\mathrm{X}}(r)$ obtained by Fourier transformation of the measured structure factor $S^{\mathrm{X}}(k)$ is not a linear combination of the functions $g_{\alpha\beta}(r)$, but for large atoms the error introduced by ignoring this fact is small.

In Figure 11.2 we show some results obtained by x-ray scattering for the carbon–carbon distribution function $g_{\mathrm{CC}}(r)$ in liquid ethylene near its triple point. Although ethylene is a polyatomic molecule, $g_{\mathrm{CC}}(r)$ resembles the pair distribution function for diatomics, as seen in both simulations and experiments. The main peak is appreciably weaker than in argon-like liquids and there is a pronounced shoulder on the large-r side. Both these features are consequences of the interference between inter- and intramolecular correlations. Simple geometry suggests that shoulders might be seen at combinations of distances such that $r_{\alpha\gamma} \approx |\sigma_{\alpha\beta} \pm L_{\beta\gamma}|$, where σ is an atomic diameter and $L_{\beta\gamma}$ is a bondlength, but they are often so smooth as to be undetectable. In the case of fused-hard sphere models of the intermolecular potential the shoulders appear as cusps in the site–site distribution functions, i.e. as discontinuities in the derivative of $g_{\alpha\beta}(r)$ with respect to r. The shoulder seen in Figure 11.2 is associated with "T-shaped" configurations of the type pictured in Figure 11.3.

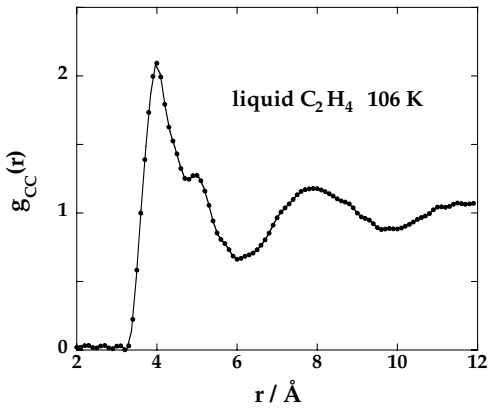

FIG. 11.2. Results obtained by x-ray scattering for the carbon–carbon distribution function in liquid ethylene. After Narten and Habenschuss.[11]

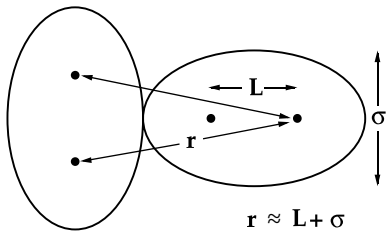

FIG. 11.3. The T-shaped configuration for a pair of homonuclear diatomics.

This particular feature is enhanced for molecules having a large quadrupole moment, such as bromine,[12] since the quadrupolar interaction strongly favours the T-configuration.

11.4 CORRELATION-FUNCTION EXPANSIONS FOR SIMPLE POLAR FLUIDS

In the simplest models of a polar fluid the intermolecular potential can be written as the sum of a small number of spherical-harmonic components. The prospects for success of theories are therefore greater than in situations where the potential contains an infinite number of harmonics and the series expansions are only slowly convergent, as is true, for example, in the case of Lennard-Jones diatomics.[4] In this section we discuss some of the general questions that arise in attempts to treat polar fluids in this way.

Consider a polar fluid for which the intermolecular potential is the same as in (1.2.4), but which we rewrite here as

$$v(1,2) = v_0(R) - \frac{\mu^2}{R^3} D(1,2) \tag{11.4.1}$$

with

$$D(1,2) = 3(\mathbf{u}_1 \cdot \mathbf{s})(\mathbf{u}_2 \cdot \mathbf{s}) - \mathbf{u}_1 \cdot \mathbf{u}_2 \tag{11.4.2}$$

where $R \equiv |\mathbf{R}_{12}|$, $\mathbf{s}$ is a unit vector in the direction of $\mathbf{R}_{12}$, $\mathbf{u}_i$ is a unit vector parallel to the dipole moment of molecule i, $v_0(R)$ is assumed to be spherically symmetric and the angle-dependent terms represent the ideal dipole–dipole interaction. It was first shown by Wertheim[13] and subsequently elaborated by others[14] that an adequate description of the static properties of such a fluid can be obtained by working with a basis set consisting of only three functions: $S(1,2) = 1$, $\Delta(1,2) = \mathbf{u}_1 \cdot \mathbf{u}_2$ and $D(1,2)$, defined above. The solution for $h(1,2)$ is therefore assumed to be of the form

$$h(1,2) = h_S(R) + h_\Delta(R)\Delta(1,2) + h_D(R)D(1,2) \tag{11.4.3}$$

On multiplying through (11.4.3) successively by S, Δ and D and integrating over angles we find that the projections $h_S(R)$, $h_\Delta(R)$ and $h_D(R)$ are given by

$$h_S(R) = \langle h(1,2) \rangle_{\Omega_1 \Omega_2} \tag{11.4.4}$$

$$h_\Delta(R) = 3\langle h(1,2)\Delta(1,2) \rangle_{\Omega_1 \Omega_2} \tag{11.4.5}$$

$$h_D(R) = \tfrac{3}{2}\langle h(1,2)D(1,2) \rangle_{\Omega_1 \Omega_2} \tag{11.4.6}$$

Equation (11.4.3) is equivalent to an expansion in laboratory-frame harmonics, since the functions Δ and D are the same, respectively, as the rotational invariants Φ^{110} and Φ^{112} introduced in (11.2.9).

The direct correlation function $c(1,2)$ can be treated in similar fashion to $h(1,2)$. We therefore write

$$c(1,2) = c_S(R) + c_\Delta(R)\Delta(1,2) + c_D(R)D(1,2) \tag{11.4.7}$$

and introduce both (11.4.3) and (11.4.7) into the molecular Ornstein–Zernike relation (11.1.4). After taking Fourier transforms we find that

$$\hat{h}(1,2) = \hat{c}(1,2) + \rho\langle \hat{c}(1,3)\hat{h}(3,2)\rangle_{\boldsymbol{\Omega}_3} \tag{11.4.8}$$

where, for example:

$$\hat{h}(1,2) = \hat{h}_S(k) + \hat{h}_\Delta(k)\Delta(1,2) + \int h_D(R)D(1,2)\exp(-i\mathbf{k}\cdot\mathbf{R})\,\mathrm{d}\mathbf{R} \tag{11.4.9}$$

The term in D can be transformed by taking the direction of $\mathbf{k}$ as the z-axis and making the substitution $\mathbf{s} = (\sin\theta\cos\phi, \sin\theta\sin\phi, \cos\theta)$. Two integrations by parts show that

$$\begin{aligned}\int_{-1}^{1}\int_{0}^{2\pi} &(\mathbf{u}_1\cdot\mathbf{s})(\mathbf{u}_2\cdot\mathbf{s})\exp(-i\mathbf{k}\cdot\mathbf{R}\cos\theta)\,\mathrm{d}\phi\,\mathrm{d}(\cos\theta)\\ &= -4\pi R^2\big(3u_{1z}u_{2z}j_2(kR) - \mathbf{u}_1\cdot\mathbf{u}_2\big[j_0(kR) + j_2(kR)\big]\big)\end{aligned} \tag{11.4.10}$$

where $j_2(x) = 3x^{-3}\sin x - 3x^{-2}\cos x - x^{-1}\sin x$. Thus

$$\int h_D(R)D(1,2)\exp(-i\mathbf{k}\cdot\mathbf{R})\,\mathrm{d}\mathbf{R} = D_k(1,2)\bar{h}_D(k) \tag{11.4.11}$$

with

$$D_k(1,2) = 3u_{1z}u_{2z} - \mathbf{u}_1\cdot\mathbf{u}_2 = \frac{3(\mathbf{u}_1\cdot\mathbf{k})(\mathbf{u}_2\cdot\mathbf{k})}{k^2} - \mathbf{u}_1\cdot\mathbf{u}_2 \tag{11.4.12}$$

and the Hankel transform $\bar{h}_D(k)$ is

$$\bar{h}_D(k) = -4\pi\int_0^\infty j_2(kR)h_D(R)R^2\,\mathrm{d}R \tag{11.4.13}$$

Equation (11.4.11) is a particular case of the general result (11.2.12); the transform of $c_D(R)D(1,2)$ is handled in the same way.

In order to summarise the effect of the angular integrations in (11.4.8), we define the angular convolution of two functions A, B as

$$A * B = B * A = \frac{1}{\Omega}\int A(1,3)B(3,2)\,\mathrm{d}\boldsymbol{\Omega}_3 \equiv \langle A(1,3)B(3,2)\rangle_{\boldsymbol{\Omega}_3} \tag{11.4.14}$$

For the functions of interest here the "multiplication" rules shown in Table 11.1 are easily established. We see from the table that the functions S, Δ and D_k form a closed set under

TABLE 11.1. *Rules for the evaluation of angular convolutions of the functions S, Δ and D_k*

	S	Δ	D_k
S	S	0	0
Δ	0	$\Delta/3$	$D_k/3$
D_k	0	$D_k/3$	$(D_k+2\Delta)/3$

the operation (11.4.14) in the sense that convolution of any two functions yields only a function in the same set (or zero). The practical significance of this result is the fact that if $h(1,2)$ is assumed to be of the form (11.4.3), then $c(1,2)$ is necessarily given by (11.4.7), and vice versa. A closure of the Ornstein–Zernike relation is still required. However, if this does not generate any new harmonics, (11.4.3) and (11.4.7) together form a self-consistent approximation, to which a solution can be found either analytically (as in the MSA, Section 11.6) or numerically.

At large R, $c(1,2)$ behaves as $-\beta v(1,2)$. Hence $c_D(R)$ must be long ranged, decaying asymptotically as R^{-3}. It turns out, as we shall see in Section 11.5, that $h_D(R)$ also decays as R^{-3}, the strength of the long-range part being related to the dielectric constant of the fluid, but the other projections of $h(1,2)$ and $c(1,2)$ are all short ranged. The slow decay of $h_D(R)$ and $c_D(R)$ creates difficulties in numerical calculations. It is therefore convenient to introduce two short-range, auxiliary functions $h_D^0(R)$ and $c_D^0(R)$. These are defined in terms, respectively, of $h_D(R)$ and $c_D(R)$ in such a way as to remove the long-range parts. Thus

$$h_D^0(R) = h_D(R) - 3\int_R^\infty \frac{h_D(R')}{R'}\,\mathrm{d}R' \tag{11.4.15}$$

with an analogous definition of $c_D^0(R)$; we see from (11.4.15) that $h_D^0(R)$ vanishes for R in the range where $h_D(R)$ has reached its asymptotic value. The inverse of (11.4.15) is

$$h_D(R) = h_D^0(R) - \frac{3}{R^3}\int_0^R h_D^0(R')R'^2\,\mathrm{d}R' \tag{11.4.16}$$

which can be checked by first differentiating (11.4.16) with respect to R and then integrating from R to $R=\infty$ (where both $h_D(R)$ and $h_D^0(R)$ are zero); this leads back to (11.4.15). Equation (11.4.16) shows that $h_D(R)$ behaves asymptotically as

$$\lim_{R\to\infty} h_D(R) = -\frac{3}{4\pi R^3}\lim_{k\to 0}\hat{h}_D^0(k) \tag{11.4.17}$$

The short-range functions $h_D^0(R)$ and $c_D^0(R)$ play an important part in the analytical solution of the MSA for dipolar hard spheres.

We have seen that use of the approximation (11.4.3) has some attractive mathematical features. The solution is of physical interest, however, only because the projections $h_S(R)$, $h_\Delta(R)$ and $h_D(R)$ contain between them all the information needed to calculate both the thermodynamic and static dielectric properties of the fluid. We postpone discussion of the

difficult problem of dielectric behaviour until the next section, but expressions for thermodynamic properties are easily derived. If $v_0(R)$ in (11.4.1) is the hard-sphere potential, the excess internal energy is determined solely by the dipole–dipole interaction and (11.1.9) becomes

$$\frac{U^{\mathrm{ex}}}{N} = -2\pi\rho \int_0^\infty \frac{\mu^2}{R_{12}} \langle D(1,2) g(1,2) \rangle_{\boldsymbol{\Omega}_1 \boldsymbol{\Omega}_2} \, \mathrm{d}R_{12}$$
$$= -\frac{4\pi\mu^2\rho}{3} \int_0^\infty \frac{h_D(R)}{R} \, \mathrm{d}R \tag{11.4.18}$$

where we have used the definition (11.4.6) and the fact that the angle average of $D(1,2)$ is zero. If $v_0(R)$ is the Lennard-Jones potential or some other spherically symmetric but continuous interaction, there will be a further contribution to U^{ex} that can be expressed as

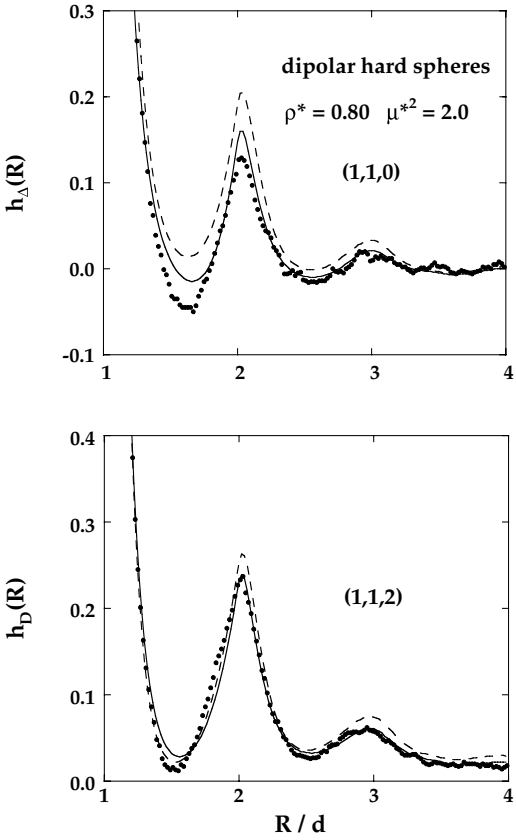

FIG. 11.4. Projections of $h(1,2)$ for a fluid of dipolar hard spheres at $\rho d^3 = 0.80$, $\beta\mu^2/d^3 = 2.0$. The points are Monte Carlo results and the curves are calculated from the LHNC (dashes) and RHNC (continuous lines) approximations discussed in Section 11.6. After Fries and Patey.[15]

an integral over $h_S(R)$. Similarly, (11.1.10) can be used to relate the equation of state to the projections $h_S(R)$ and $h_D(R)$. Thermodynamic properties are therefore not explicitly dependent on $h_\Delta(R)$.

Examples of $h_\Delta(R)$ and $h_D(R)$ for the dipolar hard-sphere fluid are shown in Figure 11.4. For the state point concerned, corresponding to a static dielectric constant ε of approximately 30, the curves retain a pronounced oscillatory character over a range of three to four molecular diameters. The structure in $h_\Delta(R)$ and $h_D(R)$ disappears as the dipole moment is reduced, but $h_S(R)$ (not shown) is much less sensitive to the value of ε and bears a strong resemblance to the pair correlation function of a fluid of non-polar hard spheres. The structure seen in the Δ and D projections is also depressed by addition of a quadrupole moment, as we discuss again in Section 11.6.

11.5 THE STATIC DIELECTRIC CONSTANT

Our goal in this section is to obtain molecular expressions for the static dielectric constant. We show, in particular, that ε is related to the long-wavelength behaviour of each of the functions $\hat{h}_\Delta(k)$ and $\bar{h}_D(k)$ introduced in the previous section.[16] By suitably combining the two results it is also possible to express ε in terms of site–site distribution functions.[17]

Consider a sample of dielectric material (a polar fluid) placed in an external electric field. Let $\mathbf{E}(\mathbf{R}, t)$ be the field at time t at a point $\mathbf{R}$ inside the sample (the Maxwell field), let $\mathbf{P}(\mathbf{R}, t)$ be the polarisation induced in the sample and let $\mathbf{E}^0(\mathbf{R}, t)$ be the field that would exist at the same point if the sample were removed (the external field). The polarisation is related to the Maxwell field by

$$\mathbf{P}(\mathbf{R}, t) = \int \mathrm{d}\mathbf{R}' \int_{-\infty}^{t} \boldsymbol{\chi}(\mathbf{R} - \mathbf{R}', t - t') \cdot \mathbf{E}(\mathbf{R}', t') \, \mathrm{d}t' \tag{11.5.1}$$

where the tensor $\boldsymbol{\chi}(\mathbf{R}, t)$ is an after-effect function of the type introduced in Section 7.6. A Fourier–Laplace transform of (11.5.1) (with z on the real axis) gives

$$\widehat{\mathbf{P}}(\mathbf{k}, \omega) = \boldsymbol{\chi}(\mathbf{k}, \omega) \cdot \widehat{\mathbf{E}}(\mathbf{k}, \omega) \tag{11.5.2}$$

where the susceptibility $\boldsymbol{\chi}(\mathbf{k}, \omega)$ is related to the dielectric permittivity $\boldsymbol{\varepsilon}(\mathbf{k}, \omega)$ by

$$\boldsymbol{\chi}(\mathbf{k}, \omega) = \frac{1}{4\pi}\big[\boldsymbol{\varepsilon}(\mathbf{k}, \omega) - \boldsymbol{I}\big] \tag{11.5.3}$$

The polarisation is also related to the external field via a second susceptibility, $\boldsymbol{\chi}^0(\mathbf{k}, \omega)$:

$$\widehat{\mathbf{P}}(\mathbf{k}, \omega) = \boldsymbol{\chi}^0(\mathbf{k}, \omega) \cdot \widehat{\mathbf{E}}^0(\mathbf{k}, \omega) \tag{11.5.4}$$

The external field and Maxwell field will not, in general, be the same, because the polarisation of the sample makes a contribution to the Maxwell field. The relation between the

two fields, and hence also that between $\boldsymbol{\chi}$ and $\boldsymbol{\chi}^0$, is dependent on sample geometry. We shall assume that the system is infinite, in which case the relation between $\mathbf{E}$ and $\mathbf{E}^0$ is

$$\mathbf{E}(\mathbf{R}, t) = \mathbf{E}^0(\mathbf{R}, t) + \int \boldsymbol{T}(\mathbf{R} - \mathbf{R}') \cdot \mathbf{P}(\mathbf{R}', t)\, \mathrm{d}\mathbf{R}' \tag{11.5.5}$$

where $\boldsymbol{T}(\mathbf{R})$ is the dipole–dipole interaction tensor defined by (1.2.5). Integrals involving the dipole–dipole tensor must be handled with care, since $\boldsymbol{T}(\mathbf{R})$ has a singularity at the origin; the usual procedure is to cut off the integrand inside a sphere of radius σ centred on the origin and take the limit $\sigma \to 0$ after integration.[18] The transform of (11.5.5) is then given by

$$\widehat{\mathbf{E}}(\mathbf{k}, \omega) = \widehat{\mathbf{E}}^0(\mathbf{k}, \omega) - \frac{4\pi}{k^2}\mathbf{k}\mathbf{k} \cdot \widehat{\mathbf{P}}(\mathbf{k}, \omega) \tag{11.5.6}$$

The relationship between the two susceptibilities follows immediately from consideration of (11.5.2), (11.5.4) and (11.5.6):[19]

$$\boldsymbol{\chi}^0(\mathbf{k}, \omega) = \left[\boldsymbol{I} + \left(4\pi/k^2\right)\mathbf{k}\mathbf{k} \cdot \boldsymbol{\chi}(\mathbf{k}, \omega)\right]^{-1} \cdot \boldsymbol{\chi}(\mathbf{k}, \omega) \tag{11.5.7}$$

It is an experimental fact that the dielectric permittivity is an intensive property of the fluid, having a value that for given $\mathbf{k}$ and ω is independent of sample size and shape. The same is therefore true of the susceptibility $\boldsymbol{\chi}(\mathbf{k}, \omega)$, since the two quantities are trivially linked by (11.5.3). It follows, provided the system is isotropic, that both $\boldsymbol{\varepsilon}$ and $\boldsymbol{\chi}$ must be independent of the direction of $\mathbf{k}$. Thus, in the limit $\mathbf{k} \to 0$:

$$\lim_{\mathbf{k}\to 0} \boldsymbol{\varepsilon}(\mathbf{k}, \omega) = \varepsilon(\omega)\boldsymbol{I}, \qquad \lim_{\mathbf{k}\to 0} \boldsymbol{\chi}(\mathbf{k}, \omega) = \chi(\omega)\boldsymbol{I} \tag{11.5.8}$$

where $\varepsilon(\omega)$ and $\chi(\omega)$ are scalars. On the other hand, the longitudinal (parallel to $\mathbf{k}$) and transverse (perpendicular to $\mathbf{k}$) components of $\boldsymbol{\chi}^0(\mathbf{k}, \omega)$ must behave differently in the long-wavelength limit; this is inevitable, given that the relation between $\boldsymbol{\chi}^{(0)}$ and $\boldsymbol{\varepsilon}$ is shape dependent. Taking the z-axis along the direction of $\mathbf{k}$, we find from (11.5.3), (11.5.7) and (11.5.8) that

$$4\pi \lim_{\mathbf{k}\to 0} \chi^0_{\alpha\alpha}(\mathbf{k}, \omega) = \varepsilon(\omega) - 1, \quad \alpha = x, y \tag{11.5.9a}$$

$$4\pi \lim_{\mathbf{k}\to 0} \chi^0_{zz}(\mathbf{k}, \omega) = \frac{\varepsilon(\omega) - 1}{\varepsilon(\omega)} \tag{11.5.9b}$$

and

$$4\pi \lim_{\mathbf{k}\to 0} \operatorname{Tr} \boldsymbol{\chi}^0(\mathbf{k}, \omega) = \frac{[\varepsilon(\omega) - 1][2\varepsilon(\omega) + 1]}{\varepsilon(\omega)} \tag{11.5.10}$$

The statistical-mechanical problem is to obtain expressions for the components of $\boldsymbol{\chi}^0$ in terms of microscopic variables. The microscopic expression for the polarisation induced

by the external field is

$$\mathbf{P}(\mathbf{R},t)=\big\langle\mathbf{M}(\mathbf{R},t)\big\rangle_{\mathbf{E}^0}=\left\langle\mu\sum_{i=1}^{N}\mathbf{u}_i(t)\delta\big[\mathbf{R}-\mathbf{R}_i(t)\big]\right\rangle_{\mathbf{E}^0} \tag{11.5.11}$$

where $\mathbf{M}(\mathbf{R},t)$ is the dipole-moment density, $\langle\cdots\rangle_{\mathbf{E}^0}$ denotes a statistical average in the presence of the external field and the other symbols have the same meaning as in earlier sections of this chapter. The susceptibility $\boldsymbol{\chi}^0$ can now be calculated by the methods of linear-response theory described in Section 7.6. (Note that $\boldsymbol{\chi}$ cannot be treated in the same way as $\boldsymbol{\chi}^0$, because the Maxwell field is not an "external" field in the required sense.) As an application of the general result given by (7.6.21) we find that

$$\boldsymbol{\chi}^0(\mathbf{k},\omega)=\frac{\beta}{V}\left(\langle\mathbf{M}_{\mathbf{k}}\mathbf{M}_{-\mathbf{k}}\rangle+i\omega\int_0^\infty\big\langle\mathbf{M}_{\mathbf{k}}(t)\mathbf{M}_{-\mathbf{k}}\big\rangle\exp(i\omega t)\,\mathrm{d}t\right) \tag{11.5.12}$$

where the statistical averages are now computed in the absence of the field, $\mathbf{M}_{\mathbf{k}}\equiv\mathbf{M}_{\mathbf{k}}(t=0)$ and

$$\mathbf{M}_{\mathbf{k}}(t)=\mu\sum_{i=1}^{N}\mathbf{u}_i(t)\exp\big[-i\mathbf{k}\cdot\mathbf{R}_i(t)\big] \tag{11.5.13}$$

If we take the limit $\omega\to0$, (11.5.12) reduces to

$$\chi^0_{\alpha\alpha}(\mathbf{k},0)=\frac{\beta}{V}\big\langle M^\alpha_{\mathbf{k}}M^\alpha_{-\mathbf{k}}\big\rangle,\quad\alpha=x,y,z \tag{11.5.14}$$

By combining this result with (11.5.10) we find that

$$\frac{(\varepsilon-1)(2\varepsilon+1)}{9\varepsilon}=g_{\mathrm{K}}y \tag{11.5.15}$$

where $\varepsilon\equiv\varepsilon(0)$ is the static dielectric constant, y is a molecular parameter defined as

$$y=\frac{4\pi\mu^2\rho}{9k_{\mathrm{B}}T} \tag{11.5.16}$$

and g_{K}, the Kirkwood "g-factor", is given by

$$g_{\mathrm{K}}=\big\langle|\mathbf{M}|^2\big\rangle/N\mu^2 \tag{11.5.17}$$

where $\mathbf{M}\equiv\mathbf{M}_{\mathbf{k}=0}$ is the total dipole moment of the sample. Equation (11.5.17) can be rewritten, with the help of (11.4.5), as

$$\begin{aligned}g_{\mathrm{K}}&=1+\big\langle(N-1)\mathbf{u}_1\cdot\mathbf{u}_2\big\rangle\\&=1+\frac{4\pi\rho}{3}\int_0^\infty h_\Delta(R)R^2\,\mathrm{d}R=1+\tfrac{1}{3}\rho\hat{h}_\Delta(0)\end{aligned} \tag{11.5.18}$$

where $h_\Delta(R)$ is the function appropriate to an infinite system.

Equation (11.5.15) is the first of two key results of this section. It was originally derived by Kirkwood[20] via a calculation of the fluctuation in total dipole moment of a spherical region surrounded by a dielectric continuum and is commonly referred to as the Kirkwood formula. By setting $g_K = 1$ we obtain the result known as the Onsager equation; this amounts to ignoring the short-range angular correlations represented by the function $h_\Delta(R)$. The Kirkwood formula could have been obtained by working throughout in the $\omega = 0$ limit, but the frequency-dependent results are needed for the discussion of dielectric relaxation in Section 11.11.

The next task is to relate ε to the function $h_D(R)$. To do this we must consider separately the longitudinal and transverse components of $\boldsymbol{\chi}^0$. For the longitudinal component we find from (11.5.13) and (11.5.14) that

$$\begin{aligned}\chi^0_{zz}(\mathbf{k},0) &= \frac{\beta}{V}\langle M^z_{\mathbf{k}} M^z_{-\mathbf{k}}\rangle \\ &= \tfrac{1}{3}\mu^2\rho\beta + \mu^2\rho\beta\big\langle (N-1)u_{1z}u_{2z}\exp(-i\mathbf{k}\cdot\mathbf{R}_{12})\big\rangle \\ &= \tfrac{1}{3}\mu^2\rho\beta \\ &\quad + \frac{\mu^2\rho^2\beta}{\Omega^2}\iiint \frac{(\mathbf{k}\cdot\mathbf{u}_1)(\mathbf{k}\cdot\mathbf{u}_2)}{k^2}h(1,2) \\ &\quad \times \exp(-i\mathbf{k}\cdot\mathbf{R}_{12})\,\mathrm{d}\mathbf{R}_{12}\,\mathrm{d}\boldsymbol{\Omega}_1\,\mathrm{d}\boldsymbol{\Omega}_2 \\ &= \tfrac{1}{3}\mu^2\rho\beta + \mu^2\rho^2\beta\big\langle k^{-2}(\mathbf{k}\cdot\mathbf{u}_1)(\mathbf{k}\cdot\mathbf{u}_2)\hat{h}(1,2)\big\rangle_{\boldsymbol{\Omega}_1\boldsymbol{\Omega}_2} \end{aligned} \tag{11.5.19}$$

We now substitute for $\hat{h}(1,2)$ from (11.4.9) and evaluate the angular averages with the help of the following, easily proved results (here $\mathbf{n}$ is a unit vector of fixed orientation):

$$\big\langle (\mathbf{n}\cdot\mathbf{u}_1)(\mathbf{n}\cdot\mathbf{u}_2)(\mathbf{u}_1\cdot\mathbf{u}_2)\big\rangle_{\boldsymbol{\Omega}_1\boldsymbol{\Omega}_2} = \big\langle (\mathbf{n}\cdot\mathbf{u}_1)^2(\mathbf{n}\cdot\mathbf{u}_2)^2\big\rangle_{\boldsymbol{\Omega}_1\boldsymbol{\Omega}_2} = \tfrac{1}{9} \tag{11.5.20}$$

A simple calculation shows that

$$\lim_{\mathbf{k}\to 0}\chi^0_{zz}(\mathbf{k},0) = \tfrac{1}{3}\mu^2\rho\beta\big[1 + \tfrac{1}{3}\rho\hat{h}_\Delta(0) + \tfrac{2}{3}\rho\bar{h}_D(0)\big] \tag{11.5.21}$$

Although we have used the approximation (11.4.9), (11.5.21) is an exact result, since the terms ignored in (11.4.9) make no contribution to the angular average in (11.5.19).

The transverse component can be treated in a similar way. It is possible, however, to take a short-cut, since we are interested only in the $\mathbf{k} \to 0$ limit. Equations (11.5.10), (11.5.15) and (11.5.18) show that the trace of the tensor $\boldsymbol{\chi}^0(\mathbf{k},\omega)$ in the long-wavelength, low-frequency limit is

$$\lim_{\mathbf{k}\to 0}\operatorname{Tr}\boldsymbol{\chi}^0(\mathbf{k},0) = \mu^2\rho\beta\big[1 + \tfrac{1}{3}\hat{h}_\Delta(0)\big] \tag{11.5.22}$$

As the two transverse components are equivalent, we find from (11.5.21) and (11.5.22) that

$$\lim_{\mathbf{k}\to 0}\chi^0_{xx}(\mathbf{k},0) = \tfrac{1}{3}\mu^2\rho\beta\big[1 + \tfrac{1}{3}\rho\hat{h}_\Delta(0) - \tfrac{1}{3}\rho\bar{h}_D(0)\big] \tag{11.5.23}$$

Use of (11.5.9) leads to the second main result:

$$\frac{(\varepsilon-1)^2}{\varepsilon} = 4\pi \lim_{\mathbf{k}\to 0}\left[\chi^0_{xx}(\mathbf{k},0) - \chi^0_{zz}(\mathbf{k},0)\right] = -3y\rho\bar{h}_D(0) \tag{11.5.24}$$

It can be shown[21] that the Hankel transform in (11.5.24) is also the Fourier transform of the short-range function $h^0_D(R)$ defined by (11.4.15), i.e. $\bar{h}_D(k) = \hat{h}^0_D(k)$. Equations (11.4.17) and (11.5.24) may therefore be combined to give

$$\lim_{R\to\infty} h_D(R) = \frac{(\varepsilon-1)^2}{4\pi y\rho\varepsilon}\frac{1}{R^3} \tag{11.5.25}$$

The calculation establishes both that $h(1,2)$ is long ranged and that the long range of the correlations is responsible for the difference in behaviour of the longitudinal and transverse components of the susceptibility $\boldsymbol{\chi}^{(0)}(\mathbf{k},0)$.

The expansion of $h(1,2)$ in terms of the functions S, $\Delta(1,2)$ and $D(1,2)$ is particularly well suited to treating the type of potential model described by (11.4.1), but its range of applicability is wider than this. It can be used, in particular, to discuss the dielectric properties of linear, interaction-site molecules. Consider a diatomic molecule of bondlength L with charges $\pm q$ located on atoms α, β and a dipole moment $\mu = qL$. If ℓ_α is the distance of atom α from the molecular centre, (11.3.4) shows that the Fourier transform of any of the atomic pair correlation functions may be written as

$$\hat{h}_{\alpha\beta}(k) = \left\langle \hat{h}(1,2)\exp(-i\mathbf{k}\cdot\mathbf{u}_1\ell_\alpha)\exp(i\mathbf{k}\cdot\mathbf{u}_2\ell_\beta)\right\rangle_{\boldsymbol{\Omega}_1\boldsymbol{\Omega}_2} \tag{11.5.26}$$

with $\ell_\alpha + \ell_\beta = L$. The plane-wave functions can be replaced by their Rayleigh expansions:[22]

$$\exp(-i\mathbf{k}\cdot\mathbf{r}) = \sum_{n=0}^{\infty}(2n+1)i^n j_n(kr)P_n(\mathbf{k}\cdot\mathbf{r}/kr) \tag{11.5.27}$$

but since our concern is only with the behaviour of $\hat{h}_{\alpha\beta}(k)$ to order k^2, it is necessary to retain only the contributions from $n=0$ and $n=1$. If, in addition, we substitute for $\hat{h}(1,2)$ from (11.4.9), (11.5.26) becomes

$$\begin{aligned}\hat{h}_{\alpha\beta}(k) = \big\langle \big(&\hat{h}_S(k) + \hat{h}_\Delta(k)\mathbf{u}_1\cdot\mathbf{u}_2 + \bar{h}_D(k)\left[3k^{-2}(\mathbf{k}\cdot\mathbf{u}_1)(\mathbf{k}\cdot\mathbf{u}_2) - \mathbf{u}_1\cdot\mathbf{u}_2\right]\big)\\ &\times\left[j_0(-k\ell_\alpha) + 3ij_1(-k\ell_\alpha)\mathbf{k}\cdot\mathbf{u}_1/k\right]\\ &\times\left[j_0(k\ell_\beta) + 3ij_1(k\ell_\beta)\mathbf{k}\cdot\mathbf{u}_2/k\right]\big\rangle_{\boldsymbol{\Omega}_1\boldsymbol{\Omega}_2}\end{aligned} \tag{11.5.28}$$

where $j_1(x) = x^{-2}\sin x - x^{-1}\cos x$.

The terms in (11.5.28) that survive the integration over angles are those of the type shown in (11.5.20). On multiplying out, integrating with the help of (11.5.20) and collecting terms we find that

$$\hat{h}_{\alpha\beta}(k) = \hat{h}_S(k)j_0(-k\ell_\alpha)j_0(k\ell_\beta) - \left[\hat{h}_\Delta(k) + 2\bar{h}_D(k)\right]j_1(-k\ell_\alpha)j_1(k\ell_\beta) \tag{11.5.29}$$

The functions $\hat{h}_{\alpha\alpha}(k)$, $\hat{h}_{\beta\alpha}(k)$ and $\hat{h}_{\beta\beta}(k)$ can be expressed in a similar way. If we now expand the Bessel functions to order k^2, the result obtained for the Fourier transform of the function $\Delta h(r)$ in (11.3.8) is

$$\Delta\hat{h}(k) = \frac{k^2L^2}{9}\left[\hat{h}_\Delta(0) + 2\bar{h}_D(0)\right] + \mathcal{O}(k^4) \tag{11.5.30}$$

or, from (11.5.9b) and (11.5.21):

$$\Delta h^{(2)} = \frac{L^2}{9\rho}\left(\frac{\varepsilon - 1}{y\varepsilon} - 3\right) \tag{11.5.31}$$

where $\Delta h^{(2)}$ is the coefficient introduced in (11.3.10). Equation (11.5.31) expresses the dielectric constant as a combination of integrals involving only the site–site distribution functions and may be rewritten as

$$\sum_\alpha \sum_\beta q_\alpha q_\beta h^{(2)}_{\alpha\beta} = \frac{\mu^2}{9\rho}\left(\frac{\varepsilon - 1}{y\varepsilon} - 3\right) \tag{11.5.32}$$

where q_α is the charge on site α. The result in this form is not limited to diatomics: it applies to any interaction-site molecule.[23]

It is clear from (11.5.18) that $\hat{h}_\Delta(0)$ is related to the angular correlation parameter (11.3.10) by $G_1 = \frac{1}{3}\rho\hat{h}_\Delta(0)$. This is true whether or not the molecule has a dipole moment, but the analysis that leads to (11.3.10) is valid only in the non-polar case. The difference between polar and non-polar molecules lies in the long-range function $h_D(R)$. The significance of $h_D(R)$ can be seen in the fact that whereas $\hat{h}_\Delta(0)$ contributes equally to the longitudinal and transverse components of the long-wavelength susceptibility $\boldsymbol{\chi}(\mathbf{k}, 0)$, $\bar{h}_D(0)$ does not. The effect of long-range correlations can therefore be suppressed by setting $\bar{h}_D(0) = 0$ in (11.5.30), which then reduces to (11.3.10).

11.6 INTEGRAL-EQUATION APPROXIMATIONS FOR DIPOLAR HARD SPHERES

The expansion of $h(1, 2)$ or $c(1, 2)$ in terms of S, $\Delta(1, 2)$ and $D(1, 2)$ was first exploited by Wertheim[13] in obtaining the analytic solution to the MSA (mean spherical approximation) for dipolar hard spheres. Although the MSA is not a quantitatively satisfactory theory, Wertheim's methods have had a considerable influence on later work on simple models of polar fluids.

The groundwork for the solution has already been laid in Section 11.4. The next stage in the calculation consists in substituting for $\hat{h}(1, 2)$ and $\hat{c}(1, 2)$ in the Ornstein–Zernike relation (11.4.8), integrating over angles with the help of Table 11.1, and equating coefficients of S, Δ and D_k on the two sides of the equation. The terms in S separate from those in Δ

and D_k to give

$$\hat{h}_S(k) = \hat{c}_S(k) + \rho\hat{c}_S(k)\hat{h}_S(k) \tag{11.6.1a}$$

$$\hat{h}_\Delta(k) = \hat{c}_\Delta(k) + \tfrac{1}{3}\rho\big[\hat{c}_\Delta(k)\hat{h}_\Delta(k) + 2\bar{c}_D(k)\bar{h}_D(k)\big] \tag{11.6.1b}$$

$$\bar{h}_D(k) = \bar{c}_D(k) + \tfrac{1}{3}\rho\big[\bar{c}_D(k)\bar{h}_D(k) + \bar{c}_D(k)\hat{h}_\Delta(k) + \hat{c}_\Delta(k)\bar{h}_D(k)\big] \tag{11.6.1c}$$

The Hankel transforms in these equations are the Fourier transforms of the short-range functions $h_D^0(R)$ and $c_D^0(R)$; this fact has already been used in the derivation of (11.5.25). The inverse Fourier transforms of $\hat{h}_S(k)$, $\hat{h}_\Delta(k)$ and $\bar{h}_D(k)$ can therefore all be written in terms of spatial convolution integrals (denoted by the symbol $\otimes$):

$$h_S(R) = c_S(R) + \rho c_S \otimes h_S \tag{11.6.2a}$$

$$h_\Delta(R) = c_\Delta(R) + \tfrac{1}{3}\rho\big(c_\Delta \otimes h_\Delta + 2c_D^0 \otimes h_D^0\big) \tag{11.6.2b}$$

$$h_D(R) = c_D(R) + \tfrac{1}{3}\rho\big(c_D^0 \otimes h_D^0 + c_D^0 \otimes h_\Delta + c_\Delta \otimes h_D^0\big) \tag{11.6.2c}$$

These equations are to be solved subject to the MSA closure relations (4.5.2). For dipolar hard spheres, (4.5.2) becomes

$$h(1,2) = -1, \quad R < d; \qquad c(1,2) = \frac{\beta\mu^2 D(1,2)}{R^3}, \quad R > d \tag{11.6.3}$$

or, equivalently:

$$\begin{aligned} h_S(R) &= -1, \quad R < d; \qquad & h_\Delta(R) = h_D(R) &= 0, \quad R < d \\ c_D(R) &= \frac{\beta\mu^2}{R^3}, \quad R > d; \qquad & c_S(R) = c_\Delta(R) &= 0, \quad R > d \end{aligned} \tag{11.6.4}$$

It is clear from (11.6.2a) and (11.6.4) that within the MSA the functions $h_S(R)$ and $c_S(R)$ are simply the solution to the PY equation for non-polar hard spheres: the dipolar interaction has no effect on the distribution of molecular centres. The closure relations involving the projections $h_D(R)$ and $c_D(R)$ can also be written as

$$h_D^0(R) = -3K, \quad R < d; \qquad c_D^0(R) = 0, \quad R > d \tag{11.6.5}$$

where K is the dimensionless parameter defined as

$$K = \int_d^\infty \frac{h_D(R)}{R}\,\mathrm{d}R \tag{11.6.6}$$

We now look for a linear combination of functions that causes (11.6.2b) and (11.6.2c) to become decoupled. Direct substitution shows that this is achieved by taking

$$\begin{aligned} h_+(R) &= \frac{1}{3K}\big[h_D^0(R) + \tfrac{1}{2}h_\Delta(R)\big] \\ h_-(R) &= \frac{1}{3K}\big[h_D^0(R) - h_\Delta(R)\big] \end{aligned} \tag{11.6.7}$$

with analogous expressions for $c_+(R)$ and $c_-(R)$. The new functions satisfy the equations

$$\begin{aligned} h_+(R) &= c_+(R) + 2K\rho c_+ \otimes h_+ \\ h_-(R) &= c_-(R) - K\rho c_- \otimes h_- \end{aligned} \tag{11.6.8}$$

Equations (11.6.8) are to be solved subject to the closure relations $h_+(R) = h_-(R) = -1$, $R < d$ (this is why the factor $1/3K$ is included in (11.6.7)) and $c_+(R) = c_-(R) = 0$, $R > d$.

The original problem has now been greatly simplified. The effect of decoupling the different projections, first in (11.6.2) and then in (11.6.8), means that the Ornstein–Zernike relation has been reduced to three independent equations, namely (11.6.2a) and (11.6.8). These equations, with their corresponding closure relations, are just the Percus–Yevick approximation for hard spheres at densities equal, respectively, to ρ, $2K\rho$ and $-K\rho$. The fact that one solution is required at a negative density poses no special difficulty.

To complete the analytical solution it is necessary to relate the quantity K to hard-sphere properties. Given the analogue of (11.4.16) for $c_D(R)$, the closure relation (11.6.5) requires that

$$c_D(R) = -\frac{3}{R^3}\int_0^d c_D^0(R')R'^2\,\mathrm{d}R', \quad R > d \tag{11.6.9}$$

Because $c_D^0(R)$ vanishes for $R > d$, comparison of (11.6.4) with (11.6.9) shows that

$$\beta\mu^2 = -3\int_0^d c_D^0(R)R^2\,\mathrm{d}R = -\frac{3}{4\pi}\bar{c}_D(0) \tag{11.6.10}$$

The function $c_D^0(R)$ may be written as

$$\begin{aligned} c_D^0(R) &= K\big[c_+(R) + c_-(R)\big] \\ &= K\big[2c_{\mathrm{PY}}(R;\,2K\rho) + c_{\mathrm{PY}}(R;\,-K\rho)\big] \end{aligned} \tag{11.6.11}$$

where $c_{\mathrm{PY}}(R;\,\rho)$ is the PY hard-sphere direct correlation function at a density ρ. Let $Q(\eta) = \beta(\partial P/\partial\rho)_T$ be the PY approximation to the inverse compressibility of the hard-sphere fluid at a packing fraction η. Integrals over $c_{\mathrm{PY}}(R;\,\rho)$ can be related to $Q(\eta)$ via the general expression (3.8.8) and the approximate result (4.4.12). A short calculation shows that

$$Q(\eta) = 1 - 4\pi\rho\int_0^d c_{\mathrm{PY}}(R;\,\rho)R^2\,\mathrm{d}R = \frac{(1+2\eta)^2}{(1-\eta)^4} \tag{11.6.12}$$

On combining the last three equations we find that

$$\beta\mu^2 = -3K\int_0^d \left[2c_{\mathrm{PY}}(R;\,2K\rho) + c_{\mathrm{PY}}(R;\,-K\rho)\right]R^2\,\mathrm{d}R$$
$$= \frac{3}{4\pi\rho}\left[Q(2K\eta) - Q(-K\eta)\right] \tag{11.6.13}$$

or

$$3y = Q(2K\eta) - Q(-K\eta) \tag{11.6.14}$$

where y is the parameter defined by (11.5.16). Equations (11.6.12) and (11.6.14) determine K implicitly for given choices of y and η; as y varies from 0 to ∞, $K\eta$ varies from 0 to $\frac{1}{2}$.

As an alternative to (11.6.12) we can write

$$\frac{1}{Q(\eta)} = 1 + 4\pi\rho\int_0^\infty h_{\mathrm{PY}}(R;\,\rho)R^2\,\mathrm{d}R \tag{11.6.15}$$

whence, from (11.6.7):

$$\rho\hat{h}_{\Delta}(0) = 8\pi\rho K\int_0^\infty \left[h_+(R) - h_-(R)\right]R^2\,\mathrm{d}R$$
$$= 8\pi\rho K\int_0^\infty \left[h_{\mathrm{PY}}(R;\,2K\rho) - h_{\mathrm{PY}}(R;\,-K\rho)\right]R^2\,\mathrm{d}R$$
$$= \frac{1}{Q(2K\eta)} + \frac{2}{Q(-K\eta)} - 3 \tag{11.6.16}$$

Taken together, (11.5.15), (11.6.14) and (11.6.16) lead to a remarkably simple expression for the dielectric constant:

$$\varepsilon = \frac{Q(2K\eta)}{Q(-K\eta)} \tag{11.6.17}$$

The same result is obtained if (11.5.24) is used instead of (11.5.15).

Although the method of solution is very elegant, comparison with the results of Monte Carlo calculations shows that the MSA does not provide a quantitatively acceptable description of the properties of the dipolar hard-sphere fluid. As is evident from comparison of (11.6.14) with (11.6.17), the dielectric constant in the MSA is dependent only on the parameter y and not separately on the two independent parameters $\rho^* = \rho d^3$ and $\mu^{*2} = \beta\mu^2/d^3$ required to specify the thermodynamic state of the system. When both these variables are large (for liquid water, $\mu^{*2} \approx 3$), use of the MSA gives values of ε that are much too small, as shown by the results in Figure 11.5.

The analytical solution to the MSA has also been found for dipolar hard-sphere mixtures[25] and for dipolar hard spheres with a Yukawa tail.[26] The numerical results obtained for dipolar mixtures show again that the MSA seriously underestimates the dielectric constant. Addition of a Yukawa term to the pair potential leads to changes in thermodynamic properties, but the dielectric constant remains the same.

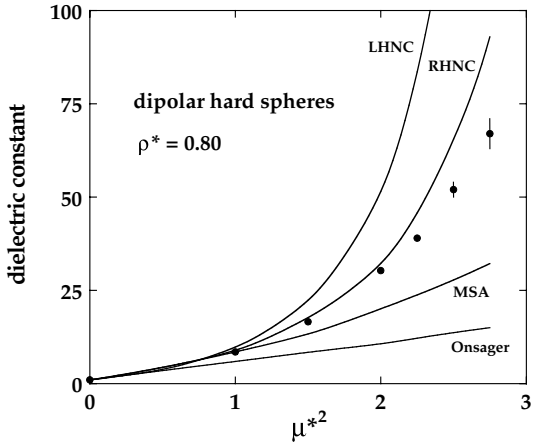

FIG. 11.5. Dielectric constant of the dipolar hard-sphere fluid at $\rho d^3 = 0.80$ as a function of $\mu^{*2} = \beta\mu^2/d^3$, showing a comparison between Monte Carlo results[24] (points) and the predictions of theories discussed in the text (curves). After Stell *et al.*[14]

Of the developments inspired by Wertheim's work on the MSA the simplest to implement is the "linearised HNC" or LHNC approximation of Patey and coworkers.[27] The LHNC approximation is equivalent to one proposed earlier by Wertheim himself and called by him the "single-superchain" approximation.[28] In the case of dipolar hard spheres the LHNC approximation resembles the MSA in basing itself on expansions of $h(1,2)$ and $c(1,2)$ limited to the terms in S, $\Delta(1,2)$ and $D(1,2)$, but improves on it by employing a closure relation that is applicable to other simple models of polar liquids, such as the Stockmayer fluid. As the name suggests, the LHNC closure corresponds to a linearisation of the HNC approximation, which in its general form is

$$c(1,2) = h(1,2) - \ln g(1,2) - \beta v(1,2) \tag{11.6.18}$$

The LHNC closure is obtained by substituting for $h(1,2)$ and $c(1,2)$ from (11.4.3) and (11.4.7) and linearising with respect to the functions Δ and D. The result is

$$\begin{aligned} c(1,2) = {} & h_S(R) - \ln g_S(R) - \beta v_0(R) + h_\Delta(R)\big[1 - 1/g_S(R)\big]\Delta(1,2) \\ & + \big(h_D(R)\big[1 - 1/g_S(R)\big] + \beta\mu^2/R^3\big)D(1,2) \end{aligned} \tag{11.6.19}$$

where $g_S(R) = h_S(R) + 1$. When $v_0(R)$ is the hard-sphere potential, (11.6.19) reduces to the MSA closure if the substitution $g_S(R) = 1$ for $R > d$ is made; the MSA may therefore be regarded as the low-density limit of the LHNC approximation.

The linearisation involved in (11.6.19) means that the closure relation involves only the harmonics S, Δ and D. This is consistent with the assumed form of $h(1,2)$ and $c(1,2)$ and the results in (11.6.2) remain valid. In other words, the relation between $h_S(R)$ and $c_S(R)$ remains independent of the other projections, and the results for these two functions are just the solutions to the HNC equation for the potential $v_0(R)$. In contrast to the MSA,

however, the projections on Δ and D are influenced by the projections on S through the appearance of $g_S(R)$ in the closure relations for $c_\Delta(R)$ and $c_D(R)$.

The method of solution of the LHNC equations for the problem of dipolar hard spheres parallels that used for the MSA up to the point at which the linear combinations (11.6.7) are introduced. In the LHNC approximation the functions $h_+(R)$, $c_+(R)$ remain coupled to $h_-(R)$, $c_-(R)$ through the closure relations; the solution must therefore be completed numerically. Some results for the projections $h_\Delta(R)$ and $h_D(R)$ are compared with those obtained by the Monte Carlo method in Figure 11.4. The general agreement between theory and simulation is fair and improves markedly as the value of the parameter μ^* is reduced. However, in contrast to the MSA, the calculated values of the dielectric constant are now everywhere too large, as is evident from Figure 11.5, and the discrepancy between theory and simulation increases rapidly with μ^*. The LHNC approximation has also been applied to systems of quadrupolar hard spheres and to fluids of hard spheres carrying both dipoles and quadrupoles.[27(b,d)] The calculations are more complicated than in the purely dipolar case because the pair potentials contain additional harmonics and still more are generated by the angular convolutions in the Ornstein–Zernike relation. The results for the mixed, dipolar–quadrupolar system are of particular interest for the light they throw on the way in which the quadrupolar interaction modifies the dipolar correlations in the fluid. The effect on the projection $h_\Delta(R)$ is particularly striking. In the purely dipolar case, when both ρ^* and μ^* are large, $h_\Delta(R)$ is positive nearly everywhere, and significantly different from zero out to values of R corresponding to ten or more molecular diameters. Since ε is determined by the integral of $R^2 h_\Delta(R)$ over all R (see (11.5.18)), these effects combine to give very large values for the dielectric constant. The addition of even a small quadrupole moment leads to a marked falling off in both the magnitude and range of $h_\Delta(R)$; ε therefore decreases rapidly as the quadrupole moment is increased. This could have been anticipated from the discussion in Section 11.3, since Δ is zero for the ideal T-shaped configurations favoured by the quadrupolar interaction.

The LHNC approximation for dipolar hard spheres resembles the MSA to the extent that the function $g_S(R)$ is the pair distribution function of the underlying hard-sphere system, and is therefore independent of the strength of the dipole–dipole interaction. This unrealistic feature disappears when the expansion of the HNC closure relation is taken to second order, since $h_S(R)$ and $c_S(R)$ can no longer be decoupled from the other projections. In other respects, the results are not always an improvement on those of the linearised version, and the theory becomes computationally more awkward to implement. Rather than pursuing the expansion to higher orders, it seems preferable to return to the full HNC closure (11.6.18) or its "reference" (RHNC) modification.[15,29] The molecular generalisation of the RHNC closure (4.7.1) is

$$\ln g(1,2) = -\beta\big[v(1,2) - k_\mathrm{B}T d_0(1,2)\big] + h(1,2) - c(1,2) \tag{11.6.20}$$

where $d_0(1,2)$ is the bridge function of some anisotropic reference system. In the case of dipolar hard spheres, however, hard spheres are the obvious choice of reference system. Because the closure relation couples together all harmonic components of $h(1,2)$ and $c(1,2)$, the results obtained depend on the number of harmonics retained when expanding the pair functions, but essentially complete convergence is achieved with a basis set of easily manageable size. Some results for $h_\Delta(R)$ and $h_D(R)$ are shown in Figure 11.4. The theoretical

curves lie systematically below those given by the LHNC approximation; the dielectric constant is therefore much reduced and the agreement with simulations correspondingly improved, as Figure 11.5 confirms.

It is known experimentally that the Kirkwood g-factors of many non-associating polar liquids are close to unity, and the very large discrepancies seen in Figure 11.5 between the Monte Carlo results and the predictions of the Onsager approximation (for which $g_K = 1$) show that the dipolar hard-sphere model gives dielectric constants that are unrealistically large.[30] The role played by quadrupolar forces provides a possible explanation of the experimental facts, but a more realistic model of a polar fluid must also make allowance for the inevitable anisotropy in the short-range, repulsive forces. The simplest such model consists of a hard, homonuclear diatomic with a dipole moment superimposed at the mid-point between the two spheres. Within the RHNC approximation the natural choice of reference system is now the underlying hard-dumbbell fluid, the bridge function of which can be calculated from the molecular version of the PY approximation.[31] The same general approach can be used for heteronuclear molecules having either soft or hard cores. Some good results have been achieved in this way, though a strong empirical element is often involved both in the choice of reference system and in the form of closure relation used to calculate the corresponding bridge function.[32]

11.7 INTERACTION-SITE DIAGRAMS

The diagrammatic expansions of $c(1,2)$, $h(1,2)$ and $y(1,2)$ given in Chapters 3 and 4 are also applicable to molecular fluids if certain minor changes in interpretation are made. First, the circles in a "molecular" diagram are associated with both the translational and orientational coordinates of a molecule and the black circles imply integrations over both sets of coordinates. Secondly, black circles carry a weight factor equal to $1/\Omega$, where Ω is defined by (11.1.3). As an illustration of these rules, the diagram

which appears at order ρ in the ρ-circle, f-bond expansion of $h(1,2)$ (see (4.6.2)) now represents the integral

$$\frac{\rho}{\Omega}\iint f(\mathbf{R}_{13}, \boldsymbol{\Omega}_1, \boldsymbol{\Omega}_3) f(\mathbf{R}_{23}, \boldsymbol{\Omega}_2, \boldsymbol{\Omega}_3)\, \mathrm{d}\mathbf{R}_3\, \mathrm{d}\boldsymbol{\Omega}_3$$

and is therefore much more complicated to evaluate than in the atomic case.

The diagrammatic expansion of $h(1,2)$ is not immediately useful in cases where the focus of interest is the set of site–site distribution functions $h_{\alpha\beta}(r)$ rather than $h(1,2)$. Ladanyi and Chandler[33] have shown how the diagrammatic approach can be adapted to the needs of such a situation and this section is devoted to a brief review of their results.

We give only a simplified treatment, restricting the detailed discussion to the case of rigid, diatomic (or two-site) molecules. The generalisation to larger numbers of interaction sites is straightforward, but requires a more complex notation.

The first step is to rewrite the molecular Mayer function $f(1,2)$ as a product of interaction-site Mayer functions $f_{\alpha\beta}(r)$:

$$\begin{aligned} f(1,2) = \exp\bigl[-\beta v(1,2)\bigr] - 1 &= \exp\biggl(-\beta \sum_{\alpha}\sum_{\beta} v_{\alpha\beta}\bigl(|\mathbf{r}_{2\beta} - \mathbf{r}_{1\alpha}|\bigr)\biggr) - 1 \\ &= -1 + \prod_{\alpha,\beta}\bigl[f_{\alpha\beta}\bigl(|\mathbf{r}_{2\beta} - \mathbf{r}_{1\alpha}|\bigr) + 1\bigr] \end{aligned} \tag{11.7.1}$$

The subscripts α, β run over all interaction sites in the molecule; if there are two sites per molecule, the right-hand side of (11.7.1) consists of 15 separate terms. Equation (11.7.1) can be used to rewrite the integrals occurring in the density expansion of $h(1,2)$. As the simplest possible example, consider the low-density limit of $h(1,2)$, namely $\lim_{\rho\to 0} h(1,2) = f(1,2)$. The corresponding approximation to, say, $h_{\alpha\alpha}(\mathbf{r},\mathbf{r}')$ is

$$\lim_{\rho\to 0} h_{\alpha\alpha}(\mathbf{r},\mathbf{r}') = \iint f(1,2)\delta(\mathbf{r}_{1\alpha} - \mathbf{r})\delta(\mathbf{r}_{2\alpha} - \mathbf{r}')\,\mathrm{d}1\,\mathrm{d}2 \tag{11.7.2}$$

When $f(1,2)$ is replaced by (11.7.1), (11.7.2) becomes

$$\begin{aligned} \lim_{\rho\to 0} h_{\alpha\alpha}(\mathbf{r},\mathbf{r}') = f_{\alpha\alpha}\bigl(|\mathbf{r}' - \mathbf{r}|\bigr) &+ \bigl[1 + f_{\alpha\alpha}\bigl(|\mathbf{r}' - \mathbf{r}|\bigr)\bigr] \\ &\times \iint \bigl[f_{\alpha\beta}\bigl(|\mathbf{r}_{2\beta} - \mathbf{r}_{1\alpha}|\bigr) + \text{six other terms}\bigr] \\ &\times \delta(\mathbf{r}_{1\alpha} - \mathbf{r})\delta(\mathbf{r}_{2\alpha} - \mathbf{r}')\,\mathrm{d}1\,\mathrm{d}2 \end{aligned} \tag{11.7.3}$$

The integrals appearing on the right-hand side of (11.7.3) can be re-expressed in terms of an intramolecular site–site distribution function $s_{\alpha\beta}(\mathbf{x}-\mathbf{y})$ defined as

$$\begin{aligned} s_{\alpha\beta}(\mathbf{x}-\mathbf{y}) &= (1-\delta_{\alpha\beta}) \int \delta(\mathbf{R}_1 + \mathbf{u}_1\ell_\alpha - \mathbf{x})\delta(\mathbf{R}_1 - \mathbf{u}_1\ell_\beta - \mathbf{y})\,\mathrm{d}1 \\ &= (1-\delta_{\alpha\beta})\bigl\langle \delta(\mathbf{x}-\mathbf{y}-\mathbf{u}_1 L)\bigr\rangle_{\boldsymbol{\Omega}_1} \\ &= \frac{(1-\delta_{\alpha\beta})}{4\pi L^2}\delta\bigl(|\mathbf{x}-\mathbf{y}| - L\bigr) \end{aligned} \tag{11.7.4}$$

where ℓ_α, ℓ_β and $\mathbf{u}_1$ have the same meaning as in (11.5.26) and $L = \ell_\alpha + \ell_\beta$. The function $s_{\alpha\beta}(\mathbf{r})$ is the probability density for finding site β of a molecule at a position $\mathbf{r}$, given that site α of the same molecule is at the origin. The definition (11.7.4) satisfies the obvious conditions that the interpretation as an intramolecular distribution function requires, i.e.

$s_{\alpha\beta}(\mathbf{r}) = s_{\beta\alpha}(\mathbf{r})$, $\mathbf{s}_{\alpha\alpha}(\mathbf{r}) = 0$ and $\int s_{\alpha\beta}(\mathbf{r})\,\mathrm{d}\mathbf{r} = 1$, $\alpha \neq \beta$. The integral shown explicitly in (11.7.3) can now be transformed as follows:

$$\begin{aligned}
&\iint \delta(\mathbf{r}_{1\alpha} - \mathbf{r})\delta(\mathbf{r}_{2\alpha} - \mathbf{r}')\, f_{\alpha\beta}\big(|\mathbf{r}_{2\beta} - \mathbf{r}_{1\alpha}|\big)\,\mathrm{d}1\,\mathrm{d}2 \\
&\quad = \int \mathrm{d}\mathbf{x} \iint \delta(\mathbf{r}_{1\alpha} - \mathbf{r})\delta(\mathbf{r}_{2\alpha} - \mathbf{r}')\, f_{\alpha\beta}(\mathbf{r}_{1\alpha} - \mathbf{x})\delta(\mathbf{r}_{2\beta} - \mathbf{x})\,\mathrm{d}1\,\mathrm{d}2 \\
&\quad = \int \mathrm{d}1\,\delta(\mathbf{r}_{1\alpha} - \mathbf{r}) \int \mathrm{d}\mathbf{x}\, f_{\alpha\beta}(\mathbf{r}_{1\alpha} - \mathbf{x}) \int \mathrm{d}2\,\delta(\mathbf{r}_{2\alpha} - \mathbf{r}')\delta(\mathbf{r}_{2\beta} - \mathbf{x}) \\
&\quad = \int f_{\alpha\beta}\big(|\mathbf{r} - \mathbf{x}|\big) s_{\alpha\beta}(\mathbf{x} - \mathbf{r}')\,\mathrm{d}\mathbf{x} \qquad (11.7.5)
\end{aligned}$$

All other integrals in (11.7.3) may be treated in the same way and each can then be represented by an *interaction-site diagram*. The circles (white or black) of an interaction-site diagram are associated with the coordinates of interaction sites and the bonds, in the two-site case, represent components of the 2×2 matrices $\boldsymbol{f}$ and $\boldsymbol{s}$ formed by the functions $\{f_{\alpha\beta}\}$ and $\{s_{\alpha\beta}\}$, respectively. The symmetry number and value of an interaction-site diagram are defined as in the atomic case (see Section 3.7), except that black circles imply a summation over all sites in the molecule in addition to integration over site coordinates. For example, if we denote an $\boldsymbol{f}$-bond by a solid line and an $\boldsymbol{s}$-bond by a broken line, the diagrammatic representation of the sum of integrals in (11.7.3) is

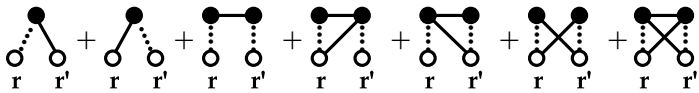

The diagrams shown all have a symmetry number of one. They are of zeroth order in density, since they arise from a molecular diagram – their "molecular origin" – that represents the low-density limit of $h(1, 2)$. Thus all circles, white or black, are 1-circles. The order in density of any interaction-site diagram in the expansion of a site–site pair correlation function is equal to the number of black circles in its molecular origin, which in turn is equal to the number of black circles in the interaction-site diagram minus the number of $\boldsymbol{s}$-bonds.

The procedure outlined above can be applied to each of the integrals appearing in the density expansion of $h(1, 2)$. This yields an expansion of any of the functions $h_{\alpha\beta}(\mathbf{r})$ in terms of interaction-site diagrams. As the example (11.7.3) demonstrates, each molecular diagram is replaced by a large number of interaction-site diagrams, but the interaction-site diagrams are mathematically simpler objects because all reference to orientational coordinates has disappeared. (Note that the black circles no longer carry the weight factor Ω^{-1} associated with the black circles of a molecular diagram.)

The topology of allowed interaction-site diagrams is restricted in certain ways. Diagrams must be simple and connected; white circles must not be connected by an $\boldsymbol{s}$-bond (because different white circles always refer to different molecules); all black circles must be intersected by at least one $\boldsymbol{f}$-bond (otherwise they contribute nothing to the intermolecular

correlations); no circle may be intersected by more than one $\boldsymbol{s}$-bond (for reasons to be explained below); and diagrams must be free of articulation circles and articulation $\boldsymbol{s}$-bonds, i.e. $\boldsymbol{s}$-bonds whose removal causes the diagram to separate into two or more components of which at least one contains no white circle. The last restriction is imposed because any such diagram would have as its molecular origin a diagram containing one or more articulation circles; as we showed in Chapters 3 and 4, the expansions of the pair functions of interest here consist entirely of irreducible diagrams.

Given the restrictions listed above, the site–site pair correlation functions may be characterised as follows:

$$h_{\alpha\beta}(\mathbf{r}_{1\alpha}, \mathbf{r}_{2\beta}) = \big[\text{all interaction-site diagrams consisting of two white 1-circles labelled } 1\alpha \text{ and } 2\beta\text{, black 1-circles, } \boldsymbol{f}\text{-bonds and } \boldsymbol{s}\text{-bonds, each diagram to be multiplied by } \rho^n\text{, where } n \text{ is the number of black circles minus the number of } \boldsymbol{s}\text{-bonds}\big] \tag{11.7.6}$$

The generalisation of this result to molecules with more than two interaction sites requires the introduction of three-body and higher-order intramolecular distribution functions. It remains true, however, that no circle may be intersected by more than one $\boldsymbol{s}$-bond or, indeed, by more than one intramolecular bond of any order. Consider the diagram shown in (a) below. For a two-site molecule such a diagram is physically meaningless, because one site is bonded to two others. But it is also not an allowed diagram even for a three-site (or larger) molecule, because the three black circles would then be linked, as in (b), by a single bond or "face", representing a three-body intramolecular distribution function.

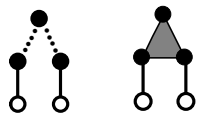

(a) (b)

The diagrammatic formalism can be extended to flexible molecules, but in that case the intramolecular distribution functions become statistically averaged quantities.

11.8 INTERACTION-SITE MODELS: THE RISM EQUATIONS

We saw in Section 11.3 that the static structure factors measured in neutron and x-ray scattering experiments on molecular liquids are weighted sums of atomic pair distribution functions. In this section we describe an integral-equation theory that has been widely used in the interpretation of diffraction experiments and, more generally, in the calculation of site–site distribution functions for interaction-site potential models: this is the "reference interaction-site model" or RISM approximation of Andersen and Chandler.[34] The theory

has been applied with particular success in calculations for model fluids composed of hard molecules. From experience with atomic systems we can expect the structure of simple molecular liquids to be dominated by the strongly repulsive part of the pair potential, and an obvious way represent to the short-range repulsions is through an interaction-site model consisting of fused hard spheres.

The key ingredient of the RISM approximation is an Ornstein–Zernike-like relation between the site–site pair correlation functions $h_{\alpha\beta}(r)$ and a set of direct correlation functions $c_{\alpha\beta}(r)$. In the atomic case the meaning of the Ornstein–Zernike relation is that the total correlation between particles 1 and 2 is the sum of all possible paths of direct correlations that propagate via intermediate particles 3, 4, ... etc. The same, intuitive idea can be applied to site-site correlations, but allowance must now be made for the fact that correlations also propagate via the intramolecular distribution functions. Hence, whereas in an atomic fluid $h(1,2)$ is given diagrammatically by the sum of all simple chains consisting of c-bonds, $h_{\alpha\beta}(r)$ consists of all simple chains formed from $\boldsymbol{c}$-bonds and $\boldsymbol{s}$-bonds. We make this idea precise by writing $h_{\alpha\beta}(r)$ as a sum of interaction-site diagrams in the form

$h_{\alpha\beta}(\mathbf{r}_{1\alpha}, \mathbf{r}_{2\beta}) =$ [all interaction-site chain diagrams consisting of two white terminal 1-circles labelled 1α and 2β, black 1-circles, at least one $\boldsymbol{c}$-bond, and $\boldsymbol{s}$-bonds, each diagram to be multiplied by ρ^{n-1}, where n is the number of $\boldsymbol{c}$-bonds]

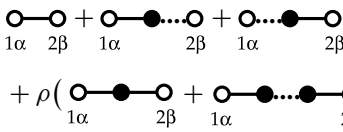

(11.8.1)

where a full line denotes a $\boldsymbol{c}$-bond and a broken line denotes an $\boldsymbol{s}$-bond. We recall that within the diagrammatic formalism a black circle implies a summation over all sites in the molecule. Thus, for example, the value of the third diagram on the right-hand side of (11.8.1) is

$$\sum_{\gamma} \int s_{\alpha\gamma}(\mathbf{r}_{1\gamma} - \mathbf{r}_{1\alpha}) c_{\gamma\beta}\big(|\mathbf{r}_{2\beta} - \mathbf{r}_{1\gamma}|\big)\, \mathrm{d}\mathbf{r}_{1\gamma}$$

The term for which $\alpha = \gamma$ contributes nothing to the sum because the intramolecular distribution function is zero when the two sites are the same.

We now have to sum the chain diagrams in (11.8.1). To do so, we use the same techniques as in Section 5.5, because the diagrams have the same topology as those in the diagrammatic expansion (5.5.16) of the renormalised potential $C(1,2)$. We define a matrix of functions $\boldsymbol{\omega}(r)$ by

$$\omega_{\alpha\beta}\big(|\mathbf{r}_{1\beta} - \mathbf{r}_{1\alpha}|\big) = \delta_{\alpha\beta}\delta(\mathbf{r}) + s_{\alpha\beta}(\mathbf{r}) \tag{11.8.2}$$

and represent $\omega_{\alpha\beta}(|\mathbf{r}_{1\beta} - \mathbf{r}_{1\alpha}|)$ by the hypervertex

Then the sum of all chain diagrams with n $\boldsymbol{c}$-bonds becomes a single diagram consisting of $(n+1)$ $\boldsymbol{\omega}$-hypervertices and n $\boldsymbol{c}$-bonds. For example:

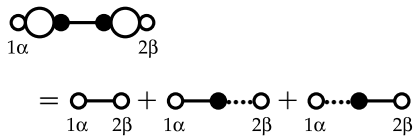

$$= \sum_{\gamma}\sum_{\delta} \iint \omega_{\alpha\gamma}\big(|\mathbf{r}_{1\alpha} - \mathbf{r}_{1\gamma}|\big) c_{\gamma\delta}\big(|\mathbf{r}_{1\gamma} - \mathbf{r}_{2\delta}|\big) \omega_{\delta\beta}\big(|\mathbf{r}_{2\delta} - \mathbf{r}_{2\beta}|\big)\, \mathrm{d}\mathbf{r}_{1\gamma}\, \mathrm{d}\mathbf{r}_{2\delta} \tag{11.8.3}$$

A hypervertex corresponds to a single molecule and incorporates all the intramolecular constraints represented by the $\boldsymbol{s}$-bonds. The Fourier transform of (11.8.3) is the $\alpha\beta$-component of the matrix $\hat{\boldsymbol{\omega}}(k) \cdot \hat{\boldsymbol{c}}(k) \cdot \hat{\boldsymbol{\omega}}(k)$, i.e.

$$\sum_{\gamma}\sum_{\delta} \hat{\omega}_{\alpha\gamma}(k)\hat{c}_{\gamma\delta}(k)\hat{\omega}_{\delta\beta}(k) = (\hat{\boldsymbol{\omega}}\hat{\boldsymbol{c}}\hat{\boldsymbol{\omega}})_{\alpha\beta} \tag{11.8.4}$$

The components of the matrix $\hat{\boldsymbol{\omega}}(k)$ are

$$\hat{\omega}_{\alpha\beta}(k) = \delta_{\alpha\beta} + (1 - \delta_{\alpha\beta}) j_0(kL_{\alpha\beta}) \tag{11.8.5}$$

where $L_{\alpha\beta}$ is the intramolecular separation of sites α, β. Similarly, the Fourier transform of the sum of all chain diagrams containing precisely n $\boldsymbol{c}$-bonds is $\rho^{n-1}((\hat{\boldsymbol{\omega}}\hat{\boldsymbol{c}})^n\hat{\boldsymbol{\omega}})_{\alpha\beta}$ (cf. (5.5.22)), and $\hat{h}_{\alpha\beta}(k)$ is the sum of a geometric series (cf. (5.5.23)). The matrix $\hat{\boldsymbol{h}}(k)$ is therefore given by

$$\hat{\boldsymbol{h}}(k) = \hat{\boldsymbol{\omega}}(k) \cdot \hat{\boldsymbol{c}}(k) \cdot \big[\boldsymbol{I} - \rho\hat{\boldsymbol{\omega}}(k) \cdot \hat{\boldsymbol{c}}(k)\big]^{-1} \cdot \hat{\boldsymbol{\omega}}(k) \tag{11.8.6a}$$

or

$$\hat{\boldsymbol{h}}(k) = \hat{\boldsymbol{\omega}}(k) \cdot \hat{\boldsymbol{c}}(k) \cdot \hat{\boldsymbol{\omega}}(k) + \rho\hat{\boldsymbol{\omega}}(k) \cdot \hat{\boldsymbol{c}}(k) \cdot \hat{\boldsymbol{h}}(k) \tag{11.8.6b}$$

Equation (11.8.6) is the Ornstein–Zernike-like relation. It can be derived in other ways than the one we have described, but the diagrammatic method[35] has a strong intuitive appeal. We shall refer to it as the RISM-OZ relation, though we shall see later that its status differs from that of the molecular Ornstein–Zernike relation (11.1.4). If $\boldsymbol{\omega}$ is the identity matrix and ρ is appropriately reinterpreted, it reduces to the Ornstein–Zernike relation for a mixture of atomic fluids.

If the RISM-OZ relation is to be useful, it must be combined with some approximate closure relation. For systems of fused hard spheres the obvious choice is a generalisation of the PY approximation for atomic hard spheres, i.e.

$$h_{\alpha\beta}(r) = -1, \quad r < d_{\alpha\beta}; \qquad c_{\alpha\beta}(r) = 0, \quad r > d_{\alpha\beta} \tag{11.8.7}$$

where $d_{\alpha\beta}$ is the $\alpha - \beta$ hard-sphere diameter. When the site–site potentials are continuous, generalisations of either the PY or HNC approximations can be used. A number of schemes have been devised for numerical solution of the resulting system of equations and calculations have been made for a wide variety of molecular liquids. Figure 11.6 shows the results of RISM calculations based on the PY closure relation for the atomic pair distribution function of a two-site Lennard-Jones model of liquid chlorine. There are some differences in detail, but all the main features seen in molecular-dynamics calculations for the same potential model are well reproduced. Note that the shoulder in the ethylene results of Figure 11.2 appears here as a well-defined subsidiary peak.

The agreement between theory and simulation seen in Figure 11.6 is typical of that achieved for other small, rigid molecules. More surprisingly, a version of the theory[37] known as "polymer" RISM or PRISM has also been applied successfully in studies of the structure of realistic models of polymer melts. Consider a chain molecule consisting of n identical monomers in a linear sequence, each represented by a single interaction site. Then, if the sites are assumed to be geometrically equivalent, the pair functions $h_{\alpha\beta}(r)$ and $c_{\alpha\beta}(r)$ are the same for all α, β and the matrix relation (11.8.6b) reduces to a single, scalar equation:

$$\hat{h}(k) = \widehat{\Omega}(k)\hat{c}(k)\widehat{\Omega}(k) + n\rho\widehat{\Omega}(k)\hat{c}(k)\hat{h}(k) \tag{11.8.8}$$

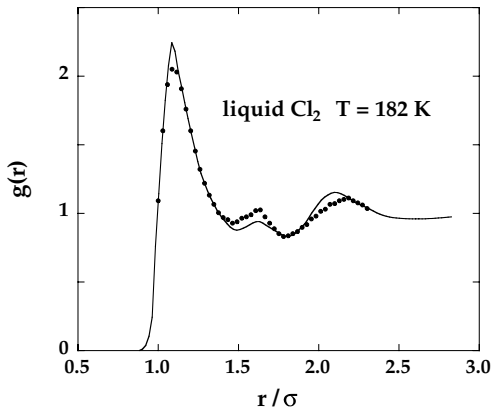

FIG. 11.6. Atom–atom distribution function for a Lennard-Jones diatomic model of liquid chlorine. The points show the results of a molecular-dynamics simulation and the curve is calculated from the RISM approximation with PY closure. After Monson.[36]

where

$$\widehat{\Omega}(k) = \frac{1}{n} \sum_{\alpha} \sum_{\beta} \hat{\omega}_{\alpha\beta}(k) \tag{11.8.9}$$

is the single-chain (or intramolecular) structure factor. This reduction in form is exact for ring polymers, but it is also a good approximation for chains if end-effects can be ignored. In either case it represents a huge simplification of the original problem, even for values of n as small as 10.

When combined with a suitable closure relation, (11.8.8) can be solved numerically to yield the site–site correlation function $h(r)$, provided the single-chain structure factor is known. In principle, intramolecular and intermolecular correlations should be calculated in a self-consistent way.[38] This complication can be avoided by treating the chains as "ideal", meaning that their average conformation is determined only by the connectivity constraints along the chain. The excluded-volume interactions between sites far apart in chemical sequence are assumed to be screened by interactions with surrounding chains.[39] For highly simplified models, such as the freely jointed chain, $\widehat{\Omega}(k)$ can be calculated analytically; for more elaborate models, it can be determined from a single-chain simulation in which the interactions are truncated at some cut-off point along the chain.

11.9 ANGULAR CORRELATIONS AND THE RISM FORMALISM

Although successful in many applications, the RISM formalism suffers from a number of defects. First, it does not lend itself readily to a calculation of the equation of state and the results obtained are thermodynamically inconsistent in the sense of Section 4.4. Secondly, calculated structural properties show an unphysical dependence on the presence of "auxiliary" sites, which are sites that label a point in the molecule but contribute nothing to the intermolecular potential. Thirdly, and most unexpectedly, trivial and incorrect results are obtained for certain quantities descriptive of angular correlations in the fluid.[40] As an example, we show below that the order parameter G_1 defined by (11.1.8) is identically zero for any asymmetric but non-polar diatomic. The only assumption made is that the site–site potentials are short ranged.

We note first that all elements of the matrix $\hat{\boldsymbol{\omega}}(k)$ defined by (11.8.5) are unity when $k = 0$. If we define a matrix $\boldsymbol{Q}$ as

$$\boldsymbol{Q} = \boldsymbol{I} - n^{-1}\hat{\boldsymbol{\omega}}(0) = \begin{pmatrix} \frac{1}{2} & -\frac{1}{2} \\ -\frac{1}{2} & \frac{1}{2} \end{pmatrix} \tag{11.9.1}$$

where n is the number of sites (here equal to two), then

$$\boldsymbol{Q} \cdot \hat{\boldsymbol{\omega}}(0) = \hat{\boldsymbol{\omega}}(0) \cdot \boldsymbol{Q} = 0 \tag{11.9.2}$$

Next we write the RISM-OZ relation (11.8.6b) in the form

$$\hat{\boldsymbol{h}}(k) = \hat{\boldsymbol{\omega}}(k) \cdot \boldsymbol{X}(k) \tag{11.9.3}$$

where

$$\boldsymbol{X}(k) = \hat{\boldsymbol{c}}(k) \cdot \left[\hat{\boldsymbol{\omega}}(k) + \rho\hat{\boldsymbol{h}}(k)\right] \tag{11.9.4}$$

Expanding $\hat{\boldsymbol{\omega}}(k)$ in powers of k, we find to order k^2 that

$$\hat{\boldsymbol{h}}(k) = \left[\hat{\boldsymbol{\omega}}(0) + k^2\boldsymbol{\omega}^{(2)} + \cdots\right] \cdot \boldsymbol{X}(k) \tag{11.9.5}$$

If multiplied on the left by $\boldsymbol{Q}$, (11.9.5) reduces, by virtue of the property (11.9.2), to

$$\boldsymbol{Q} \cdot \hat{\boldsymbol{h}}(k) = \boldsymbol{Q} \cdot \left[k^2\boldsymbol{\omega}^{(2)} + \cdots\right] \cdot \boldsymbol{X}(k) \tag{11.9.6}$$

We now suppose that $\hat{\boldsymbol{h}}(k)$ and $\hat{\boldsymbol{c}}(k)$ (and hence also $\boldsymbol{X}(k)$) have small-k expansions at least up to order k^2. This is plausible, since the site–site potentials are assumed to be short ranged. Then

$$\boldsymbol{Q} \cdot \left[\hat{\boldsymbol{h}}(0) + k^2\boldsymbol{h}^{(2)} + \cdots\right] = \boldsymbol{Q} \cdot \left[k^2\boldsymbol{\omega}^{(2)} + \cdots\right] \cdot \left[\boldsymbol{X}(0) + k^2\boldsymbol{X}^{(2)} + \cdots\right] \tag{11.9.7}$$

and by equating coefficients of k^2 we find that

$$\boldsymbol{Q} \cdot \boldsymbol{h}^{(2)} = \boldsymbol{Q} \cdot \boldsymbol{\omega}^{(2)} \cdot \boldsymbol{X}(0) \tag{11.9.8}$$

We have seen in Section 11.3 that all elements of $\hat{\boldsymbol{h}}(0)$ are the same and related to the compressibility by (11.3.6). Thus $\boldsymbol{X}(0)$ may be written as

$$\boldsymbol{X}(0) = \left[1 + \rho\hat{h}_0(0)\right]\hat{\boldsymbol{c}}(0) \cdot \hat{\boldsymbol{\omega}}(0) \tag{11.9.9}$$

where $\hat{h}_0(0)$ (a scalar) is any element of $\hat{\boldsymbol{h}}(0)$. Inserting (11.9.9) in (11.9.8), multiplying on the right by $\boldsymbol{Q}$, and using again the property (11.9.2), we find that

$$\boldsymbol{Q} \cdot \boldsymbol{h}^{(2)} \cdot \boldsymbol{Q} = 0 \tag{11.9.10}$$

But every element of the matrix $\boldsymbol{Q} \cdot \boldsymbol{h}^{(2)} \cdot \boldsymbol{Q}$ is proportional to $\Delta h^{(2)}$, where $\Delta h(r)$ is defined by (11.3.8). Thus $\Delta h^{(2)} = 0$ and hence, from (11.3.10), $G_1 = 0$. As we pointed out in Section 11.3, this result is obvious on symmetry grounds for a homonuclear molecule, but in the general case it will be true (unless accidentally) only in the ideal-gas limit. Similarly, by considering terms of order k^4 in (11.9.7), it can be that $G_2 = 0$ for an asymmetric, linear, triatomic molecule.

If the molecule is polar, with the interaction sites carrying point charges, the problem becomes more complicated. When expanding $\hat{\boldsymbol{c}}(k)$, allowance must be made for a term in k^{-2}, corresponding to an r^{-1} decay of the site–site potential. This term must be treated separately, but it is then possible to show that for any interaction-site molecule

$$\rho \sum_{\alpha} \sum_{\beta} q_\alpha q_\beta h_{\alpha\beta}^{(2)} = -\frac{y\mu^2}{1+3y} \tag{11.9.11}$$

where q_α is the charge carried by site α. Comparison of (11.9.11) with the exact result (11.5.32) shows that within the RISM approximation

$$\varepsilon = 1 + 3y \tag{11.9.12}$$

which is a well-known result for the dielectric constant of an ideal gas of polar molecules.

The results in (11.9.10) and (11.9.12) are consequences solely of the RISM-OZ relation (11.8.6). They are independent of the choice of closure relation except insofar as the latter must be consistent with the assumed small-k behaviour of $\hat{\boldsymbol{h}}(k)$ and $\hat{\boldsymbol{c}}(k)$. It follows that the RISM-OZ relation, when combined with a conventional closure approximation, cannot describe correctly certain long-wavelength properties of molecular systems, of which G_1, G_2 and ε are important examples.

Attempts to develop a more satisfactory theory have developed along two different lines. The first relies on treating the RISM-OZ relation as providing the definition of the site–site direct correlation functions. So far as the calculation of angular order parameters is concerned, it then appears necessary to abandon the assumption that $c_{\alpha\beta}(r)$ is a short-range function, even when the corresponding site–site potential is short ranged. For example,[41] a non-zero value of G_1 for a symmetric diatomic is obtained if $c_{\alpha\beta}(r)$ is assumed to decay as r^{-1}. In such circumstances the concept of "direct correlation" no longer has a clear physical meaning. In the alternative approach the view is taken that the RISM-OZ relation, though plausible, does not provide an adequate basis for a complete theory of interaction-site models of molecular liquids. Accordingly, it is there rather than in the closure relation that improvement must be sought.[42] The argument is based on the difference in diagrammatic structure between the RISM-OZ relation and the molecular Ornstein–Zernike relation (11.1.4). In the latter case the indirect correlation function $b(1,2) = h(1,2) - c(1,2)$ is given, as in (4.6.1), by the sum of all simple chain diagrams containing two or more c-bonds. In any such diagram, every black circle is a nodal circle, and $c(1,2)$ consists of the subset of diagrams in the ρ-circle, f-bond expansion of $h(1,2)$ that are free of nodal circles. By analogy, it might be supposed that the $\boldsymbol{c}$-bonds in (11.8.1) represent the subset of diagrams in the expansion of $h_{\alpha\beta}(r)$ that are free of nodal circles. This is not the case. For example, the diagram

which appears at zeroth order in the density expansion of $h_{\alpha\beta}(r)$ is a diagram without nodal circles. If this is substituted into the second and third diagrams on the right-hand side of (11.8.1), it yields, respectively, diagrams (a) and (b) below:

(a) (b)

Diagram (a) is a diagram in the exact expansion of $h_{\alpha\beta}(r)$, but (b) is not. In fact, (b) is not even an allowed diagram, because two $\boldsymbol{s}$-bonds intersect the same black circle. Chandler

and coworkers[42] have shown how this problem can be overcome through the introduction of another Ornstein–Zernike-like relation that reduces to (11.8.6) in the limit $\rho \to 0$ but in which the direct correlation functions correspond to well-defined subsets of diagrams in $\boldsymbol{h}$. Calculations based on the new relation lead to non-trivial results for the angular order parameters and dielectric constant when approximate closures of conventional type are employed. However, the theory has not been widely applied, and so far as the description of short-range order is concerned it is not clear that the method represents an improvement on the original formulation.[43]

11.10 ASSOCIATING LIQUIDS

Although hydrogen-bonded liquids and other associating fluids are not normally classed as "simple", our understanding of the link between the macroscopic properties of such systems and their behaviour at the microscopic level has improved greatly in recent years. This is a development to which both experiment and simulation have made major contributions. For understandable reasons, much of the effort has been focused on studies of water. The particular geometry of the water molecule gives rise to structural features in the liquid that are not seen for other small, hydrogen-bonded species, and the macroscopic properties of water display a number of anomalies that are directly attributable to hydrogen bonding, of which the best known is the fact that the density at atmospheric pressures passes through a maximum at a temperature of 4 °C. One of the most important advances on the experimental front has been the resolution of significant differences that had previously existed between the results of x-ray and neutron-scattering measurements of the structure of liquid water. X-ray scattering is sensitive primarily to the oxygen–oxygen correlations,[44] while neutron scattering is the main source of information on correlations involving hydrogen atoms.[45] Figure 11.7 shows the results obtained by x-ray scattering for the distribution function of oxygen atoms in water at room temperature, contrasting these with the results for liquid argon already shown in Chapter 2. To assist comparison, the horizontal axis is scaled so as to bring the two main peaks into coincidence. Clearly the structure is very different in the two liquids. Two features in particular stand out. First, the area under the main peak is significantly smaller for water than it is for argon, leading to a large reduction in the nearest-neighbour coordination number defined in Section 2.5, from approximately 12 for argon to about four for water. Secondly, the oscillations in the two curves are out of phase. The second peak for water is displaced inwards with respect to that for argon and appears at a distance $r/r_{\max} = 1.61 \pm 0.01$, which is very close to the value found for the ratio of the second-neighbour separation to that of first neighbours in the ideal ice structure, i.e. $2\sqrt{(2/3)} \approx 1.63$. Both the value of the coordination number and the position of the second peak in the oxygen–oxygen distribution function provide clear evidence that the molecules in liquid water form a hydrogen-bonded network which represents a strained version of the tetrahedral ordering found in ice.

A similar picture to that outlined above emerges from the many simulations of water that have been carried out.[48] Such calculations provide a level of detail that cannot be matched experimentally concerning the number, energies and lifetimes of the hydrogen bonds formed by individual molecules. A very large number of empirical intermolecular

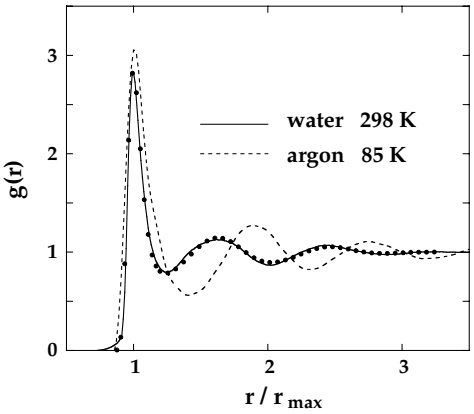

FIG. 11.7. Experimental results for the pair distribution function for oxygen atoms in water at room temperature (from x-ray scattering[44]) and for liquid argon near its triple point (from neutron scattering[46]). The points are the results for $g_{OO}(r)$ obtained by Monte Carlo calculations[47] for an interaction-site model of water. The quantity r_{max} is the separation at which the corresponding experimental curve has its main peak: 2.74 Å for water and 3.68 Å for argon.

potentials have been designed for use in simulations, which differ from each other mainly in the way in which the electrostatic interaction between molecules is described. The majority are based on rigid charge distributions represented by three or more point charges, though a number of polarisable models have also been developed, and the best of these empirical potentials give results in impressive agreement with experiment for a wide range of properties. An example of what can be achieved is illustrated by the Monte Carlo results shown in Figure 11.7. These were obtained with a model[47] (TIP5P) consisting of a Lennard-Jones interaction centred on the oxygen atom and four rigid charges, one on each hydrogen site and two at sites chosen to represent the lone-pair electrons. The same model is also successful in reproducing the density anomaly at 4 °C, while a predecessor (TIP4P) has been shown to capture all the main features of the experimental phase diagram.[49]

A number of standard, integral-equation approximations have been used in calculations for models of specific hydrogen-bonded liquids, including water,[50] but progress has also been achieved in the development of a general approach to the theory of associating fluids.[51–53] One of the most successful of these theories is that of Wertheim, which in its commonly used form has the character of a thermodynamic perturbation theory.[53(b)] The theory is designed for application to a class of highly simplified models in which the associating species are treated as particles with repulsive cores in which a number of attractive interaction sites are embedded; it is at these sites that association occurs. In the examples discussed below the particles are taken to be hard spheres of diameter d and the association sites are represented by off-centre, square-well potentials with a well-depth ε_A. Because hard spheres cannot overlap, the square-well potential can always be made sufficiently short ranged that the formation of more than one bond at any given site is forbidden, as in the example shown in Figure 11.8. A model with one association site describes a dimerising fluid; with two sites, illustrated in the figure, the spheres can form chains and rings;

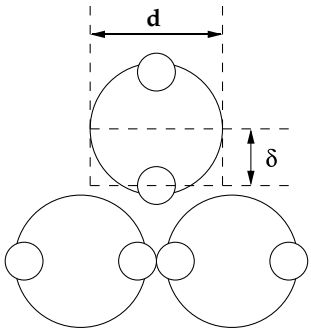

FIG. 11.8. A simple interaction-site model of an associating liquid. The large circles represent hard spheres and the small circles represent square-well interaction sites displaced from the centre of the hard sphere by a distance δ. The range of the square-well potential is sufficiently short to ensure that multiple bonding at any association site is forbidden, since that would require hard spheres to overlap.

with three sites, chain branching and network formation become possible; and a sphere with four, tetrahedrally disposed sites serves as a crude model of a water molecule.

If the attractive interactions between particles are sufficiently strong to promote association, we cannot expect a conventional perturbation calculation to succeed. In Wertheim's approach this difficulty is circumvented by treating different association aggregates as distinct species, each described by a separate single-particle density within a "multi-density" formalism. The theory leads ultimately to an expression for the free energy in terms of the densities of particles in different bonding states. As a specific example, consider the case of a system of hard spheres with a single association site. Since only dimer formation is allowed, the total number density of spheres can be written as

$$\rho = \rho_{\mathrm{M}} + 2\rho_{\mathrm{D}} \tag{11.10.1}$$

where ρ_{M} and ρ_{D} are the number densities of monomers and dimers, respectively. Diagrammatic arguments along the general lines of those pursued in Section 3.8 can then be used to show that

$$\rho = \rho_{\mathrm{M}} + \rho_{\mathrm{M}}^2 \int g_{\mathrm{MM}}(1,2)\, f_{\mathrm{A}}(1,2)\, \mathrm{d}2 \tag{11.10.2}$$

where $g_{\mathrm{MM}}(1,2)$ is the pair distribution function of the free monomers and $f_{\mathrm{A}}(1,2)$ is the Mayer function for the association potential.

The starting point in the derivation of (11.10.2) is the activity expansion of $\ln \Xi$ provided by (3.8.3). By decomposing the Mayer function for the full pair potential in the form

$$f(1,2) = f_0(1,2) + \Phi(1,2), \quad \Phi(1,2) = e_0(1,2)\, f_{\mathrm{A}}(1,2) \tag{11.10.3}$$

where $e_0(1,2)$ and $f_0(1,2)$ are, respectively, the Boltzmann factor and Mayer function for the hard-sphere potential, the right-hand side of (3.8.3) can be written a sum of diagrams consisting of z^*-circles, f_0-bond and Φ-bonds. The assumption that multiple bonding at a

single site is blocked by steric effects means that many of the diagrams either vanish or are cancelled by other diagrams; this greatly simplifies the subsequent analysis. The diagrammatic representation of the total single-particle density $\rho^{(1)}(1)$ is again obtained from the prescription given by (3.8.4), i.e. as the sum of all topologically distinct diagrams obtained from $\ln \Xi$ by whitening a black circle and labelling it 1. Now, however, the diagrams that contribute to $\rho^{(1)}(1)$ can be divided into two classes:

$$\rho^{(1)}(1) = \rho_{\mathrm{M}}^{(1)}(1) + \rho_{\mathrm{A}}^{(1)}(1) \tag{11.10.4}$$

where $\rho_{\mathrm{M}}^{(1)}(1)$ is the density of unassociated spheres (monomers) and $\rho_{\mathrm{A}}^{(1)}(1)$ is the density of spheres that form part of an associated aggregate, which in the present case can only be a dimer; the class of monomer diagrams consists of those diagrams in which the white circle is not intersected by a Φ-bond. The last step in the derivation involves a topological reduction in which the z^*-circles in the z^*-expansion of $\ln \Xi$ are replaced by $\rho^{(1)}$ or $\rho_{\mathrm{M}}^{(1)}$-circles, which in turn leads to expressions for the free energy and pressure as functionals of the two densities. The monomer density is not a free parameter; it is determined self-consistently by a relation between $\rho^{(1)}(1)$ and $\rho_{\mathrm{M}}^{(1)}(1)$, which in the homogeneous limit reduces to (11.10.2).

The full calculation is too lengthy to reproduce here, but the brief sketch we have given is enough to show that the derivation of the expression that relates ρ and ρ_{M} does not rely on the assumption that the association potential is in some sense weak. However, for the purposes of evaluating the integral in (11.10.2), the characteristic approximation of first-order perturbation theory can now be made, whereby the unknown function $g_{\mathrm{MM}}(1,2)$ in (11.10.2) is replaced by the pair distribution function of the underlying hard-sphere system, $g_0(1,2)$. Thus

$$\rho \approx \rho_{\mathrm{M}} + \rho_{\mathrm{M}}^2 \int g_0(1,2)\, f_{\mathrm{A}}(1,2)\, \mathrm{d}2 \equiv \rho_{\mathrm{M}} + \rho_{\mathrm{M}}^2 D(\rho, T) \tag{11.10.5}$$

It can then be shown that the change in free energy due to dimerisation, F^{A}, is given, to the same order in perturbation theory, by a very simple formula:

$$\frac{\beta F^{\mathrm{A}}}{N} = \frac{\beta F}{N} - \frac{\beta F_0}{N} = \ln x + \tfrac{1}{2}(1-x) \tag{11.10.6}$$

where F_0 is the free energy of the reference system and $x = \rho_{\mathrm{M}}/\rho$ is the fraction of spheres that remain unassociated. The value of x is given by the positive root of the equation obtained by dividing (11.10.5) though by ρ:

$$x^2 \rho D(\rho, T) + x - 1 = 0 \tag{11.10.7}$$

Since the association potential is very short ranged, the integral $D(\rho, T)$ can be adequately approximated in the form

$$D(\rho, T) \approx g_0(d) \int f_{\mathrm{A}}(1,2)\, \mathrm{d}2 \equiv g_0(d) D'(T) \tag{11.10.8}$$

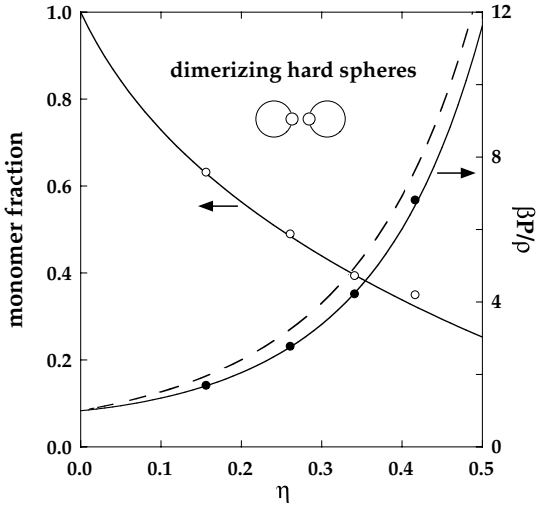

FIG. 11.9. Equilibrium composition and equation of state of a dimerising hard-sphere fluid at a reduced inverse temperature $\varepsilon_A/k_BT = 7$, where ε_A is the depth of the square-well potential. The points are the results of Monte Carlo calculations and the full curves are obtained by perturbation theory. The broken curve shows the Carnahan–Starling equation of state for the hard-sphere reference system. After Jackson *et al.*[54]

where $g_0(d)$ is the value of the hard-sphere distribution function at contact. Once the free energy is known, other thermodynamic properties can be obtained by differentiation. Figure 11.9 shows results obtained for the equilibrium composition and equation of state as a function of the hard-sphere packing fraction at a temperature such that $\varepsilon_A/k_BT = 7$. The agreement between theory and simulation is very good.

The final results of the theory and, in particular, the self-consistency of (11.10.5) and (11.10.6), can be made plausible by considering the simplest possible case, that of a dimerising ideal gas.[55] In the low-density limit, (11.10.5) reduces to[56]

$$\rho = \rho_M + \rho_M^2 \int e_0(1,2)\, f_A(1,2)\, d2 \equiv \rho_M + \rho_M^2 \Delta(T) \tag{11.10.9}$$

The role of the association potential is limited to that of dimer formation and the free energy of the partly associated system is that of a ideal gas composed of monomers and dimers. At equilibrium, the chemical potential of a sphere must be the same in its monomer and dimer states and therefore equal to $k_BT \ln \rho_M \Lambda^3$, and the pressure is $k_BT(\rho_M + \rho_D)$. A short calculation shows that the free energy $F = N\mu - PV$ of the associated system relative to that of the ideal monomeric gas is

$$\frac{\beta F^A}{V} = \rho \ln \frac{\rho_M}{\rho} + \tfrac{1}{2}(\rho - \rho_M) \tag{11.10.10}$$

which is equivalent to (11.10.6). At equilibrium, F^A must be a minimum with respect to variations in ρ_M at constant ρ, subject to the constraint imposed by (11.10.9). If we replace

the second term on the right-hand side of (11.10.10) by $(\rho - \rho_M) - \frac{1}{2}\rho_M^2 \Delta(T)$, we find that

$$\frac{\beta}{V}\frac{\partial F^A}{\partial \rho_M} = \frac{\rho}{\rho_M} - 1 - \rho_M \Delta(T) \tag{11.10.11}$$

which vanishes when (11.10.9) is satisfied. Equations (11.10.9) and (11.10.10) are therefore mutually consistent.

An important feature of Wertheim's approach is that it leads naturally to a theory of polymerisation.[57] This extension of the theory is easily illustrated, in a non-rigorous way, for the case of dimer formation. The degree of dimerisation approaches unity as the depth of the square-well potential is increased to values appropriate to a covalent bond and the Mayer function $f_A(1,2)$ becomes correspondingly large. Equation (11.10.7) implies that as the limit of complete dimerisation is approached, the monomer fraction must vanish as $x \to 1/[\rho D(\rho, T)]^{1/2}$. If we adopt the approximation (11.10.8), we find that the free energy of association in the limit $\rho \to 2\rho_D$ is

$$\frac{\beta F^A}{N} \approx -\tfrac{1}{2}\ln \rho D'(T) + \tfrac{1}{2} \tag{11.10.12}$$

implying that the equation of state of the fully dimerised system, i.e. a fluid of hard diatomics, is

$$\beta(P - P_0) = -\beta\frac{\partial F^A}{\partial V} = -\tfrac{1}{2}\rho\left(1 + \rho g_0(d)\frac{\partial \ln g_0(d)}{\partial \rho}\right) \tag{11.10.13}$$

where P_0 is the pressure of the hard-sphere fluid. If the Carnahan–Starling equation of state is used for P_0, the contact value $g_0(d)$ is given by

$$g_0(d) = \frac{\left(1 - \frac{1}{2}\eta\right)}{(1-\eta)^3} \tag{11.10.14}$$

and (11.10.13) (with $\rho = 2\rho_D$) becomes

$$\frac{\beta P}{\rho_D} = \frac{2(1 + \eta + \eta^2 - \eta^3)}{(1-\eta)^3} - \frac{\left(1 + \eta - \frac{1}{2}\eta^2\right)}{(1-\eta)\left(1 - \frac{1}{2}\eta\right)} \tag{11.10.15}$$

Equation (11.10.15) proves to be remarkably accurate. It yields results that agree with those of simulations of systems of tangent hard spheres to within 0.15% over the full density range.[57(a)]

Wertheim's theory and its extensions provide the basis for the general approach called "statistical associating fluid theory" or SAFT, within which equations of state have been developed for a wide range of complex fluids of importance in chemical engineering.[58]

11.11 REORIENTATIONAL TIME-CORRELATION FUNCTIONS

The description of the dynamical properties of molecular liquids differs most obviously from that used for atomic systems through the appearance of a class of reorientational time-correlation functions. We end this chapter by briefly considering some of the properties of these functions, limiting ourselves mainly to the case of linear molecules. We consider first the simpler problem of the single-molecule functions, leaving until later the question of collective reorientational properties.

Reorientation of a linear molecule can be described in a compact way through the introduction of a family of time-correlation functions defined as

$$C^{(l)}(t) = \left\langle P_l\left[\mathbf{u}_i(t)\cdot\mathbf{u}_i\right]\right\rangle \tag{11.11.1}$$

where, as before, $\mathbf{u}_i$ is a unit vector parallel to the internuclear axis of molecule i and $P_l(\cdots)$ is again a Legendre polynomial. The functions $C^{(l)}(t)$ are time-dependent generalisations of the angular order parameters G_l of Section 11.1. Apart from their application to linear molecules, they are also the most important functions for the description of the reorientational motion of spherical-top molecules, i.e. those in which all three principal moments of inertia are the same (CCl_4, SF_6, etc.), and of the reorientation of the main symmetry axis of symmetric-top molecules, i.e. those in which two of the principal moments of inertia are equal (NH_3, CH_3I, etc.). The $l = 1$ and $l = 2$ functions are related to the spectral bandshapes measured in infrared absorption ($l = 1$) and Raman or depolarised light scattering ($l = 2$) experiments. Information on the correlation functions can be obtained by Fourier transformation of the experimental spectra, but the interpretation of the results is complicated by a number of factors, including uncertainty about the contributions to the spectra from vibrational relaxation and collision-induced effects or, in the case of depolarised light scattering, the importance of angular correlations of the type described by the order parameter G_2.

Figure 11.10 shows some typical results for the $l = 2$ function, derived from spectroscopic measurements on carbon dioxide in two very different thermodynamic states and, in the inset, liquid acetonitrile. Under liquid-state conditions the function is approximately exponential in form, except at short times, but at low densities oscillations appear; infrared-absorption experiments on polar molecules give qualitatively similar results for the $l = 1$ function. The oscillations seen at low densities can be understood by considering the behaviour of the correlation functions in the ideal-gas limit. Let $\boldsymbol{\omega} = \mathbf{u}\times\dot{\mathbf{u}}$ be the angular velocity of a linear molecule of moment of inertia I. In the absence of any interactions the angular velocity is a constant of the motion, and in a time t the molecule will rotate through an angle $\omega t = \cos^{-1}\mathbf{u}(t)\cdot\mathbf{u}(0)$, where $\omega \equiv |\boldsymbol{\omega}|$. The probability that a molecule will rotate through such an angle is therefore determined by the probability that its angular velocity lies in the range $\omega \to \omega + \mathrm{d}\omega$. Thus the correlation function $C^{(l)}(t)$ is the value of $P_l(\cos\omega t)$ averaged over a Maxwell–Boltzmann distribution of angular velocities and appropriately normalised, i.e.

$$C^{(l)}(t) = \frac{I}{k_\mathrm{B}T}\int_0^\infty P_l(\cos\omega t)\exp\left(-\tfrac{1}{2}\beta I\omega^2\right)\omega\,\mathrm{d}\omega \tag{11.11.2}$$

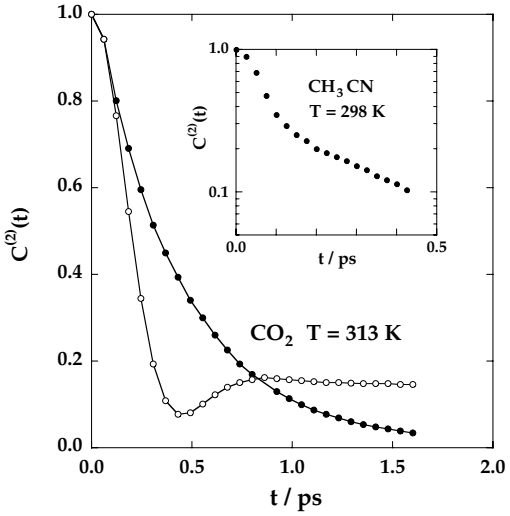

FIG. 11.10. The $l = 2$ reorientational correlation function derived from experiments on liquid and gaseous carbon dioxide (main figure) and liquid acetonitrile (inset, plotted on a logarithmic scale). Open and closed circles in the main figure show the results for $\rho/\rho_c = 0.09$ and $\rho/\rho_c = 2.35$, respectively, where ρ_c is the critical density. After Versmold[59] and Bien *et al.*[60]

These functions are oscillatory and tend to zero as $t \to \infty$ only for odd l. They are commonly called the "free-rotor" correlation functions and the oscillations seen in gas-phase experimental results are the remnants of free-rotor behaviour. Similar results are obtained for the free-rotor functions of non-linear molecules; the principle of the calculation is the same, but the final expressions have a more complicated form.[61]

The short-time expansion of the Legendre polynomial in (11.11.2) begins as

$$P_l(\cos\omega t) = 1 - \tfrac{1}{4}l(l+1)\omega^2 t^2 + \cdots \tag{11.11.3}$$

If we expand the correlation function in powers of t:

$$C^{(l)}(t) = 1 - M_2^{(l)}\frac{t^2}{2!} + \cdots \tag{11.11.4}$$

a simple integration shows that

$$M_2^{(l)} = l(l+1)\frac{k_B T}{I} \tag{11.11.5}$$

At sufficiently short times a molecule rotates freely. Hence, although (11.11.5) has been derived only in the free-rotor limit, it is also valid for interacting molecules; there is an analogy here with the short-time behaviour of the mean-square translational displacement. From the general properties of time-correlation functions discussed in Section 7.1 it follows that the coefficient $M_2^{(l)}$ is the second moment of the power spectrum of $C^{(l)}(t)$. The

mean-square width of the experimental bandshape is therefore independent of the molecular interactions. The fourth moment, however, contains a contribution proportional to the mean-square torque acting on the molecule.

The quasi-exponential behaviour of the correlation functions at high densities can be explained by invoking an approximation similar in spirit to the Langevin equation (7.3.21). We begin by writing a memory-function equation for $C^{(l)}(t)$ and taking the Laplace transform to give

$$\widetilde{C}^{(l)}(\omega) = \frac{1}{-i\omega + \widetilde{N}^{(l)}(\omega)} \tag{11.11.6}$$

From (11.11.5) it follows that the memory function $N^{(l)}(t)$ behaves as

$$N^{(l)}(t) = l(l+1)\left(\frac{k_{\mathrm{B}}T}{I}\right)n^{(l)}(t) \tag{11.11.7}$$

with $n^{(l)}(0) = 1$. We now suppose that reorientation occurs as the result of a succession of small, uncorrelated steps. This is the Debye approximation or "small-step-diffusion" model. In memory-function language the Debye approximation is equivalent to the assumption that $\widetilde{N}^{(l)}(\omega)$ is independent of frequency. To preserve the l-dependence contained in the exact result (11.11.7) we approximate the memory function in the form $\widetilde{N}^{(l)} \approx l(l+1)D_R$, where D_R (a frequency) is a "rotational-diffusion coefficient". Then

$$C^{(l)}(t) = \exp\bigl[-l(l+1)D_R t\bigr] \tag{11.11.8}$$

In this approximation the correlation functions decay exponentially at all times and for all values of l, and the entire family of functions is characterised by the single parameter D_R; for small molecules under triple-point conditions, D_R is typically of order $10^{11}\,\mathrm{s}^{-1}$. The characteristic decay times for different values of l are related by the simple rule

$$\frac{\tau_l}{\tau_{l+1}} = \frac{l+2}{l} \tag{11.11.9}$$

The correlation times derived from infrared and Raman measurements should therefore be in the ratio $\tau_1/\tau_2 = 3$. This is approximately true of many liquids and also of correlation times obtained by simulation.[62]

A weakness of the Debye approximation is its neglect of the fact that molecules rotate freely at short times. It therefore cannot account for the quadratic time dependence of the reorientational correlation functions at small t. A more complete theory must also describe correctly the details of the transition to the long-time, quasi-exponential behaviour. In the case of acetonitrile, for example, the transition region is characterised by a marked change in slope of the curve of $\ln C^{(2)}(t)$ versus t. The behaviour in the different time regimes can be described in a unified way by relating the form of the reorientational correlation functions to that of the angular-velocity autocorrelation function $C_\omega(t)$.[63] By analogy with (7.2.6) and (7.2.7) we define the rotational-diffusion coefficient of a linear

molecule as

$$D_R = \frac{k_B T}{I} \lim_{t\to\infty} \int_0^t \left(1 - \frac{s}{t}\right) C_\omega(s)\,\mathrm{d}s \tag{11.11.10}$$

where

$$C_\omega(t) = \frac{\langle \boldsymbol{\omega}_i(t)\cdot\boldsymbol{\omega}_i\rangle}{\langle|\boldsymbol{\omega}_i|^2\rangle} = \frac{I}{2k_B T}\langle \boldsymbol{\omega}_i(t)\cdot\boldsymbol{\omega}_i\rangle \tag{11.11.11}$$

Then substitution of (11.11.10) in (11.11.8) gives an expression for $C^{(l)}(t)$ in terms of $C_\omega(t)$:

$$\ln C^{(l)}(t) = -l(l+1)\left(\frac{k_B T}{I}\right)\int_0^t (t-s)C_\omega(s)\,\mathrm{d}s \tag{11.11.12}$$

The main merit of this approximation is the fact that it contains the correct short-time behaviour yet goes over to the Debye model at long times. Let τ_ω be the integral correlation time for the angular velocity, i.e.

$$\tau_\omega = \int_0^\infty C_\omega(t)\,\mathrm{d}t \tag{11.11.13}$$

At times $t \ll \tau_\omega$, $C_\omega(t) \approx 1$ and (11.11.12) becomes

$$\ln C^{(l)}(t) \approx -l(l+1)\left(\frac{k_B T}{I}\right)\frac{t^2}{2} \tag{11.11.14}$$

in agreement with the exact result (11.11.5). In the opposite limit, $t \gg \tau_\omega$, (11.11.12) becomes

$$\ln C^{(l)}(t) \approx -l(l+1)\left(\frac{k_B T}{I}\right)\tau_\omega t \tag{11.11.15}$$

which is equivalent to the Debye approximation (11.11.8) with the identification $D_R = (k_B T/I)\tau_\omega$. Finally, the behaviour at intermediate times can be related to the shape of the function $C_\omega(t)$. Differentiating (11.11.12) twice with respect to t we find that

$$\frac{\mathrm{d}^2 \ln C^{(l)}(t)}{\mathrm{d}t^2} = -l(l+1)\left(\frac{k_B T}{I}\right)C_\omega(t) \tag{11.11.16}$$

The angular-velocity autocorrelation function is not measurable experimentally, but molecular-dynamics calculations show that for liquids such as acetonitrile, in which the intermolecular torques are strong, it decays rapidly at short times and then becomes negative.[62] The change in sign occurs because the direction of the angular-velocity vector is on average soon reversed; the behaviour is similar to that seen in the linear-velocity autocorrelation function at high densities and low temperatures (see Figure 7.1). Equation (11.11.16) shows that a change in sign of $C_\omega(t)$ corresponds to a point of inflexion in $\ln C^{(l)}(t)$ of the type visible in Figure 11.10, which in turn is a common feature of the reorientational correlation functions of high-torque fluids.

A variety of theoretical schemes have been devised to treat those cases in which the Debye model is inadequate. Many of these are expressible in terms of simple approximations for the relevant memory functions, but none has proved to be satisfactory either for any large group of molecules or for any particular molecule over a wide range of density and temperature. The failure to develop an adequate theory is striking in view of the apparent simplicity in structure of the correlation functions themselves.

We have focused until now on the reorientational motion of single molecules. There are, in addition, a number of collective reorientational correlation functions that are of experimental significance and are also many-particle generalisations of single-particle functions. It is therefore of interest to establish an approximate relation between the corresponding collective and single-particle functions and, in particular, between the two correlation times, since this allows a connection to be made between the results of very different experiments. We take as an example the collective motions that determine the frequency-dependent dielectric behaviour of a polar fluid,[16] as described by the complex dielectric permittivity $\varepsilon(\omega)$ introduced in Section 11.5. The quantities of interest in the study of dielectric relaxation are the correlation functions and associated power spectra of the longitudinal (l) and transverse (t) components of the dipole-moment density (11.5.13), i.e.

$$C_l(k,t) = \frac{\langle M^z_{\mathbf{k}}(t) M^z_{-\mathbf{k}} \rangle}{\langle |M^z_{\mathbf{k}}|^2 \rangle}, \qquad C_t(k,t) = \frac{\langle M^x_{\mathbf{k}}(t) M^x_{-\mathbf{k}} \rangle}{\langle |M^x_{\mathbf{k}}|^2 \rangle} \tag{11.11.17}$$

where we have followed the usual convention that $\mathbf{k}$ is parallel to the z-axis. The functions $C_l(k,t)$ and $C_t(k,t)$ are collective analogues, generalised to non-zero k, of the single-molecule function $C^{(1)}(t)$. It follows from (11.5.9) and (11.5.12) that the long-wavelength limits of the Laplace transforms $\widetilde{C}_l(k,\omega)$ and $\widetilde{C}_t(k,\omega)$ are related to $\varepsilon(\omega)$ by

$$\begin{aligned} \frac{4\pi\beta}{V} \lim_{\mathbf{k}\to 0} \langle |M^z_{\mathbf{k}}|^2 \rangle \big[1 + i\omega \widetilde{C}_l(k,\omega)\big] &= \frac{\varepsilon(\omega) - 1}{\varepsilon(\omega)} \\ \frac{4\pi\beta}{V} \lim_{\mathbf{k}\to 0} \langle |M^x_{\mathbf{k}}|^2 \rangle \big[1 + i\omega \widetilde{C}_t(k,\omega)\big] &= \varepsilon(\omega) - 1 \end{aligned} \tag{11.11.18}$$

We begin by writing memory-function equations for $C_l(k,t)$ and $C_t(k,t)$ in the form

$$\widetilde{C}_l(k,\omega) = \frac{1}{-i\omega + \widetilde{N}_l(k\cdot\omega)}, \qquad \widetilde{C}_t(k,\omega) = \frac{1}{-i\omega + \widetilde{N}_t(k\cdot\omega)} \tag{11.11.19}$$

The initial values of the memory functions $N_l(k,t)$ and $N_t(k,t)$ in the limit $k \to 0$ can be deduced from the general property (9.1.29) and the limiting behaviour described by (11.11.18), taken for $\omega = 0$:

$$\begin{aligned} \lim_{\mathbf{k}\to 0} N_l(k, t=0) &= \lim_{\mathbf{k}\to 0} \frac{\langle |\dot{M}^z_{\mathbf{k}}|^2 \rangle}{\langle |M^z_{\mathbf{k}}|^2 \rangle} = \frac{4\pi\beta\varepsilon}{3V(\varepsilon - 1)} \langle |\dot{\mathbf{M}}|^2 \rangle \\ \lim_{\mathbf{k}\to 0} N_t(k, t=0) &= \lim_{\mathbf{k}\to 0} \frac{\langle |\dot{M}^x_{\mathbf{k}}|^2 \rangle}{\langle |M^x_{\mathbf{k}}|^2 \rangle} = \frac{4\pi\beta}{3V(\varepsilon - 1)} \langle |\dot{\mathbf{M}}|^2 \rangle \end{aligned} \tag{11.11.20}$$

where $\varepsilon \equiv \varepsilon(0)$ and $\dot{\mathbf{M}} \equiv \dot{\mathbf{M}}_{\mathbf{k}\to 0}$. In deriving these results we have exploited the fact that the different components of $\langle|\dot{\mathbf{M}}_{\mathbf{k}}|^2\rangle$ (unlike those of $\langle|\mathbf{M}_{\mathbf{k}}|^2\rangle$) are equivalent and, in particular, that $\lim_{\mathbf{k}\to 0}\langle|\dot{M}^{\alpha}_{\mathbf{k}}|^2\rangle = \frac{1}{3}\langle|\dot{\mathbf{M}}|^2\rangle$, where $\alpha = x$, y or z.

The form of (11.11.20) makes it convenient to write the memory functions at long wavelengths as

$$\lim_{\mathbf{k}\to 0}\widetilde{N}_l(k,\omega) = \frac{\varepsilon\widetilde{R}_l(\omega)}{\varepsilon - 1}, \qquad \lim_{\mathbf{k}\to 0}\widetilde{N}_t(k,\omega) = \frac{\widetilde{R}_t(\omega)}{\varepsilon - 1} \tag{11.11.21}$$

It is clear from comparison of (11.11.20) with (11.11.21) that $R_l(t=0) = R_t(t=0) = (4\pi\beta/3V)\langle|\dot{\mathbf{M}}|^2\rangle$. More generally, if the two parts of (11.11.18) are to be consistent with each other in the sense of giving the same result for $\varepsilon(\omega)$, some straightforward algebra shows that $R_l(t)$ and $R_t(t)$ must be the same for all t. Thus

$$R_l(t) = R_t(t) = R(t), \quad \text{say} \tag{11.11.22}$$

This has the immediate consequence that in the long-wavelength limit the correlation times for the longitudinal and transverse functions differ by a factor ε, i.e. $\lim_{\mathbf{k}\to 0}\widetilde{C}_l(k,0)/\widetilde{C}_t(k,0) = \varepsilon^{-1}$ or

$$\lim_{\mathbf{k}\to 0}\int_0^{\infty} C_l(k,t)\,\mathrm{d}t = \frac{1}{\varepsilon}\lim_{\mathbf{k}\to 0}\int_0^{\infty} C_t(k,t)\,\mathrm{d}t \tag{11.11.23}$$

The diffusion approximation analogous to (11.11.8) now corresponds to setting

$$R(t) = R(0)\delta(t) = \frac{4\pi\beta}{3V}\langle|\dot{\mathbf{M}}|^2\rangle\delta(t) \tag{11.11.24}$$

so that both $\widetilde{N}_l(k,\omega)$ and $\widetilde{N}_t(k,\omega)$ are assumed to be independent of frequency in the limit $\mathbf{k}\to 0$. If we define a characteristic time τ_{D} as

$$\tau_{\mathrm{D}} = \frac{3V}{4\pi\beta}\frac{\varepsilon - 1}{\langle|\dot{\mathbf{M}}|^2\rangle} \tag{11.11.25}$$

it follows from (11.11.19) and (11.11.21) that

$$\lim_{\mathbf{k}\to 0} C_l(k,t) = \exp(-\varepsilon t/\tau_{\mathrm{D}}), \qquad \lim_{\mathbf{k}\to 0} C_t(k,t) = \exp(-t/\tau_{\mathrm{D}}) \tag{11.11.26}$$

which represents a special case of the general result in (11.11.23). Simulations of strongly polar fluids confirm that the longitudinal and transverse correlation functions at small $\mathbf{k}$ do decay on very different timescales and that the ratio of correlation times is approximately equal to the value of ε derived from fluctuations in the mean-square dipole moment of the sample.[64] The transverse function is also approximately exponential in form with a decay time only weakly dependent on $\mathbf{k}$, in qualitative agreement with (11.11.26), but the longitudinal function has oscillations at large t; to describe these oscillations it is necessary

to allow for some frequency dependence of the memory function. The approximation for $\varepsilon(\omega)$ corresponding to (11.11.26) is

$$\frac{\varepsilon(\omega)-1}{\varepsilon(0)-1}=\frac{1}{1-i\omega\tau_{\mathrm{D}}} \tag{11.11.27}$$

This is an expression much used in the analysis of experimental data on $\varepsilon(\omega)$, in which context τ_{D} is invariably called the Debye relaxation time. A feature of the approximation is the fact that the curve, or Cole–Cole plot, of the real versus imaginary part of $\varepsilon(\omega)$ is a semicircle with a maximum at a frequency such that $\omega\tau_{\mathrm{D}}=1$. Many real liquids have Cole–Cole plots that are approximately semicircular. Because of its neglect of short-time, inertial effects, the diffusion approximation is least satisfactory at high frequencies, where the deviations from (11.11.27) are mostly to be found. However, as in the case of the single-molecule problem, it has proved difficult to develop an alternative theory having a wide range of applicability.

One goal of dielectric-relaxation theory is to relate the decay times that characterise the collective functions (11.11.17) and the single-molecule correlation function $C^{(1)}(t)$. The necessary link can be established by postulating some relationship between the memory functions $R(t)$ and $N^{(1)}(t)$. A simple but useful result is obtained by supposing that the two memory functions have the same time dependence, but also have their correct initial values. It follows from (9.1.29) that

$$N^{(1)}(0)=\left\langle|\dot{\mathbf{u}}_i|^2\right\rangle=\frac{\langle|\dot{\mathbf{M}}|^2\rangle}{N\mu^2}=\frac{R(0)}{3y} \tag{11.11.28}$$

where y is the molecular parameter defined by (11.5.16). If, for simplicity, we adopt the diffusion model, we find immediately from the definition (11.11.25) that

$$\tau_{\mathrm{D}}=\left(\frac{\varepsilon-1}{3y}\right)\tau_1 \tag{11.11.29}$$

or, after substitution from the Kirkwood formula (11.5.15):

$$\tau_{\mathrm{D}}=\left(\frac{3\varepsilon g_K}{2\varepsilon+1}\right)\tau_1 \tag{11.11.30}$$

This expression relates the dielectric relaxation time to the correlation time measured by infrared spectroscopy in a form determined solely by static dielectric properties of the fluid.

NOTES AND REFERENCES

1. Gray, C.G. and Gubbins, K.E., "Theory of Molecular Fluids". Clarendon Press, Oxford, 1984, p. 151.
2. Steele, W.A., *J. Chem. Phys.* **39**, 3197 (1963).
3. For a discussion of the properties of the spherical harmonics and their use in liquid-state theory, see ref. 1, particularly Appendix A.

4. See, e.g., Streett, W.B. and Tildesley, D.J., *Proc. Roy. Soc. A* **355**, 239 (1977).
5. The general procedure is described by Høye, J.S. and Stell, G., *J. Chem. Phys.* **66**, 795 (1977).
6. Sullivan, D.E. and Gray, C.G., *Mol. Phys.* **42**, 443 (1981).
7. A correction for the effects of nuclear vibration is also usually made.
8. Narten, A.H., Johnson, E. and Habenschuss, A., *J. Chem. Phys.* **73**, 1248 (1980).
9. X-ray scattering from methane is a special case. See Habenschuss, A., Johnson, E. and Narten, A.H., *J. Chem. Phys.* **74**, 5234 (1981).
10. Weis, J.J. and Levesque, D., *Phys. Rev. A* **13**, 450 (1976).
11. Narten, A.H. and Habenschuss, A., *J. Chem. Phys.* **75**, 3072 (1981).
12. (a) Narten, A.H., Agrawal, R. and Sandler, S.I., *Mol. Phys.* **35**, 1077 (1978). (b) Agrawal, R., Sandler, S.I. and Narten, A.H., *Mol. Phys.* **35**, 1087 (1978).
13. Wertheim, M.S., *J. Chem. Phys.* **55**, 4291 (1971).
14. See, e.g., Stell, G., Patey, G.N. and Høye, J.S., *Adv. Chem. Phys.* **48**, 183 (1981).
15. Fries, P.H. and Patey, G.N., *J. Chem. Phys.* **82**, 429 (1985).
16. We follow in outline the arguments of Madden, P.A. and Kivelson, D., *Adv. Chem. Phys.* **56**, 467 (1984).
17. (a) Høye, J.S. and Stell, G., *J. Chem. Phys.* **65**, 18 (1976). (b) Chandler, D., *J. Chem. Phys.* **67**, 1113 (1977).
18. Ramshaw, J.D., *J. Chem. Phys.* **70**, 1577 (1979).
19. Note the similarity with the relation (10.4.11) between the external and screened susceptibilities of charged fluids.
20. Kirkwood, J.G., *J. Chem. Phys.* **7**, 911 (1939).
21. Høye, J.S., Lebowitz, J.L. and Stell, G., *J. Chem. Phys.* **61**, 3253 (1974).
22. See ref. 1, p. 527.
23. The same result follows directly from the Stillinger–Lovett sum rules (10.2.17). See Martin, P.A., *Rev. Mod. Phys.* **60**, 1075 (1988).
24. Weis, J.J., unpublished results.
25. Cummings, P.T. and Blum, L., *J. Chem. Phys.* **85**, 6658 (1986).
26. Henderson, D., Boda, D., Szalai, I. and Chan, K.Y., *J. Chem. Phys.* **110**, 7348 (1999).
27. (a) Patey, G.N., *Mol. Phys.* **34**, 427 (1977). (b) Patey, G.N., *Mol. Phys.* **35**, 1413 (1978). (c) Patey, G.N., Levesque, D. and Weis, J.J., *Mol. Phys.* **38**, 219 (1979). (d) Patey, G.N., Levesque, D. and Weis, J.J., *Mol. Phys.* **38**, 1635 (1979).
28. Wertheim, M.S., *Mol. Phys.* **26**, 1425 (1973).
29. Lee, L.Y., Fries, P.H. and Patey, G.N., *Mol. Phys.* **55**, 751 (1985).
30. The dipolar hard-sphere model has other unsatisfactory features. See Teixeira, P.I.C., Tavares, J.M. and Telo da Gama, M.M., *J. Phys. Condens. Matter* **12**, R4111 (2000).
31. (a) Lado, F., *Mol. Phys.* **47**, 283 (1982). (b) Lado, F., Lombardero, M., Enciso, E., Abascal, J.L.F. and Lago, S., *J. Chem Phys.* **85**, 2916 (1986). (c) Lomba, E., Lombardero, M. and Abascal, J.L.F., *J. Chem. Phys.* **91**, 2581 (1989).
32. See, e.g., Lombardero, M., Martin, C., Lomba, E. and Lado, F., *J. Chem. Phys.* **104**, 6710 (1996).
33. Ladanyi, B.M. and Chandler, D., *J. Chem. Phys.* **62**, 4308 (1975).
34. Andersen, H.C. and Chandler, D., *J. Chem. Phys.* **53**, 547 (1970).
35. Chandler, D., *Mol. Phys.* **31**, 1213 (1976).
36. Monson, P.A., *Mol. Phys.* **47**, 435 (1982).
37. Schweizer, K.S. and Curro, J.G., *Phys. Rev. Lett.* **58**, 246 (1987). For a review, see Schweizer, K.S. and Curro, J.G., *Adv. Chem. Phys.* **98**, 1 (1997). The same formalism can be used for systems other than polymers: see Harnau, L. and Hansen, J.P., *J. Chem. Phys.* **116**, 9051 (2002).
38. Schweizer, K.S., Honnell, K.G. and Curro, J.G., *J. Chem. Phys.* **96**, 3211 (1992).
39. Rubinstein, M. and Colby, R.H., "Polymer Physics". Oxford University Press, Oxford, 2003. Note that the assumption of ideality is made solely for the purpose of computing the single-chain structure factor.
40. This remarkable fact was first pointed out by Chandler, D., *Faraday Disc. Chem. Soc*. **66**, 74 (1978) and later expanded upon by Sullivan and Gray, ref. 6. The derivation given in the text follows the method of Sullivan and Gray. See also Morriss, G.P. and Perram, J.W., *Mol. Phys.* **43**, 669 (1981).
41. Cummings, P.T. and Stell, G., *Mol. Phys.* **46**, 383 (1982). For later work on closure of the RISM-OZ relation, see, e.g., Raineri, F.O. and Stell, G., *J. Phys. Chem. B* **105**, 11880 (2001).

42. (a) Chandler, D., Silbey, R. and Ladanyi, B.M., *Mol. Phys.* **46**, 1335 (1982). (b) Chandler, D., Joslin, C.G. and Deutch, J.M., *Mol. Phys.* **47**, 871 (1982). (c) Chandler, D. and Richardson, D.M., *J. Phys. Chem.* **87**, 2060 (1983). See also Rossky, P.J. and Chiles, R.A., *Mol. Phys.* **51**, 661 (1984).
43. See, e.g., Reddy, G., Lawrence, C.P., Skinner, J.L. and Yethiraj, A., *J. Chem. Phys.* **119**, 13012 (2003).
44. Sorensen, J.M., Hura, G., Glaeser, R.M. and Head-Gordon, T., *J. Chem. Phys.* **113**, 9149 (2000).
45. Soper, A.K., *Chem. Phys.* **258**, 121 (2000).
46. Yarnell, J.L., Katz, M.J., Wenzel, R.G. and Koenig, S.H., *Phys. Rev. A* **7**, 2130 (1973).
47. Mahoney, M.W. and Jorgensen, W.L., *J. Chem. Phys.* **112**, 8910 (2000). TIP5P is one of a series of "transferable intermolecular potentials" devised for the simulation of water in different environments.
48. For a review, see Guillot, B., *J. Mol. Liq.* **101**, 219 (2002).
49. Sanz, E., Vega, C., Abascal, J.L.F. and MacDowell, L.G., *Phys. Rev. Lett.* **92**, 255701 (2004).
50. See, e.g., ref. 45 and Lombardero, M., Martin, C., Jorge, S., Lado, F. and Lomba, E., *J. Chem. Phys.* **110**, 1148 (1999).
51. (a) Andersen, H.C., *J. Chem. Phys.* **59**, 4714 (1973). (b) Andersen, H.C., *J. Chem. Phys.* **61**, 4985 (1974).
52. Cummings, P.T. and Stell, G., *Mol. Phys.* **51**, 253 (1984).
53. (a) Wertheim, M.S., *J. Stat. Phys.* **35**, 19 (1984). (b) Wertheim, M.S., *J. Stat. Phys.* **35**, 35 (1984).
54. Jackson, G., Chapman, W.G. and Gubbins, K.E., *Mol. Phys.* **65**, 1 (1988).
55. Galindo, A., Burton, S.J., Jackson, G., Visco, D.P. and Kofke, D.A., *Mol. Phys.* **100**, 2241 (2002).
56. Equation (11.10.9) can also be derived from the virial expansion via a calculation of the equilibrium constant for the dimerisation process. See Hill, T.L., "Introduction to Statistical Thermodynamics". Addison-Wesley, Reading, 1960, Sect. 15.3.
57. (a) Wertheim, M.S., *J. Chem. Phys.* **85**, 2929 (1986). (b) Wertheim, M.S., *J. Chem. Phys.* **87**, 7323 (1987). (c) Chapman, W.G., Jackson, G. and Gubbins, K.E., *Mol. Phys.* **65**, 1057 (1988).
58. For a review, see Müller, E.A. and Gubbins, K.E., *Ind. Eng. Chem. Res.* **40**, 2193 (2001).
59. Versmold, H., *Mol. Phys.* **43**, 383 (1981).
60. Bien, T., Possiel, M., Döge, G., Yarwood, J. and Arnold, K.E., *Chem. Phys.* **56**, 203 (1981).
61. St Pierre, A.G. and Steele, W.A., *Mol. Phys.* **43**, 123 (1981).
62. See, e.g., Madden, P.A. and Tildesley, D.J., *Mol. Phys.* **48**, 129 (1983).
63. Lynden-Bell, R.M. and McDonald, I.R., *Mol. Phys.* **43**, 1429 (1981).
64. Pollock, E.L. and Alder, B.J., *Phys. Rev. Lett.* **46**, 950 (1981).